ELSEVIER

Contents lists available at ScienceDirect

Journal of Building Engineering

journal homepage: http://www.elsevier.com/locate/jobe





Estimating surface temperature from thermal imagery of buildings for accurate thermal transmittance (U-value): A machine learning perspective

Debanjan Sadhukhan^a, Sai Peri^a, Niroop Sugunaraj^a, Avhishek Biswas^a, Daisy Flora Selvaraj^a, Katelyn Koiner^a, Andrew Rosener^a, Matt Dunlevy^b, Neena Goveas^a, David Flynn^c, Prakash Ranganathan^{a,*}

- ^a School of Electrical Engineering and Computer Science University of North Dakota, Grand Forks, ND, USA
- b SkySkopes Inc, Grand Forks, ND, USA
- ^c Department of Economics & Finance, University of North Dakota, Grand Forks, ND, USA

ARTICLE INFO

Keywords: Infrared thermography Instance segmentation UAS U-value

ABSTRACT

Thermal performance assessment of building(s) is an essential process for optimal energy management, heat-loss evaluation, and energy audit applications. Such an assessment can help foresee the requirements for future intervention(s) and aid in benchmarking energy performance. This paper provides a review of several thermal performance assessment techniques and a broad classification based on measurement types, methods, and applications. Moreover, the article provides a comprehensive survey of various quantitative indices utilized for practical heat-loss assessment of building elements. This paper's unique contribution is the proposed three-layer framework that details the handling and processing of UAS-based thermal imagery for heat loss quantification. Primarily, the novelty of this work lies in the application of an instance segmentation technique (Mask R-CNN) to compute the thermal transmittance values (e.g., U-values) for various objects (e.g., doors, walls, windows, and facades). To the best of our knowledge, this research work is first-of-its-kind using a sizeable thermal data repository (e.g. 100,000 augmented images). Multiple standard U-values are analyzed for windows and walls and compared with The American Society of Heating, Refrigerating, and Air-conditioning Engineers (ASHRAE) building standards. The preliminary results of Mask-RCNN from over 100,000 trained (including augmented) images from multiple campus buildings yield the following performance metrics: 1) provides an Average Precision (AP) of 0.67 (windows) and 0.46 (facades); and 2) Intersection of Union (IoU) of 0.05 (windows) and 0.5 (facades) respectively. Moreover, the U-values are consistently close enough to the ASHRAE standards in distinguishing window types (e.g. 0.77 for single-pane windows and 0.38 for double-pane windows).

1. Introduction

The energy management of a building is primarily driven by the heating or cooling requirements. Sustainable energy management in buildings requires minimization of heating or cooling loss. This loss often takes place across through various elements of the building such as walls, roofs or windows [1–3]. Assessing the thermal performance of these building elements is crucial for efficient energy management operations. These assessment techniques can be divided into qualitative and quantitative approaches.

The qualitative assessment of buildings using thermal images captured by Infrared (IR) cameras mounted over Unmanned Aerial Vehicles (UAVs) has been successful in detecting moisture, cracks,

insulation quality, and air leakage. In this technique, IR cameras are used to evaluate the overall thermal performance of the entire building (mostly outdoor environments). IR thermography-based approaches are gaining attention in the literature due to their ease-of-use, less cost, time, and efforts. Availability of affordable IR cameras and the use of UAVs has the potential to revolutionize the process of thermal assessment for buildings.

In quantitative measurements, heat loss is typically quantified using indices such as the heat transmittance coefficient (U-value) or thermal resistance. The U-value is defined as the rate of heat flow across one sq. meter of a surface when there is a temperature difference of one Kelvin between the inside and outside surfaces. The U-value is measured in W/m^2K or BTU/°Fft²hr. The thermal resistance or R-value is defined as the

E-mail address: prakash.ranganathan@und.edu (P. Ranganathan).

^{*} Corresponding author.

Table 1 Nomenclature.

Acronym	Definitions	Symbols	Definitions
ASTM	American Society for Testing and Material	l_{xa}	Pixel length without thermal bridges (m)
CAL	Calculating value based using Data sheet	L	Height of the wall (m)
CED	Canny Based Edge Detection	k	Proportionality constant($W/(m^2-K)$)
CEN	European Committee for Standardization	k_c	Thermal conductivity of the fluid $(Wm^{-1}K^{-1})$
CFD	Computational Fluid Mechanics	N	Number of zones
DCI DCM	Dominant Color Isolation Dominant Color Masking	N P_r	Number of pixels in IR image Prandtl number
FN	False Negatives	Q _{cur k}	Heat loss in the k^{th} zone
FP	False Positives	$q_{density}$	Heat flow rate per unit area (Wm^{-2})
GHP	Guarded Hot Plate	$q_{o,s}$	Outgoing heat flow rate per unit area (Wm^{-2})
HFM	Heat Flux Meter	Q_{iD}	Heat flow without thermal bridge (Wm^{-2})
HPT	Heating Pulse Thermography	q_{xTB}	Difference between heat flow rate with and without thermal bridge for pixel x (W/m^2)
IR	Infrared	q_x	Heat flow rate of pixel x with thermal bridge (Wm^{-2})
ISO	International Standard Organization	q_{xa}	Heat flow rate of pixel x without thermal $bridge(Wm^2)$
LT	Local Thermography	Q_{tb}	Heat flow with thermal bridge(Wm^{-2})
MEAS	Measured using HFM	R.	Thermal resistance $((m^2 - K)/W)$
ND	North Dakota	R_{si}	Internal resistance ($(m^2 - K)/W$) Internal surface thermal resistance of the air boundary layers ($m^2 - K/W$)
NDT	Non-Destructive Testing	R_{se}	External surface thermal resistance of the air boundary layers ($m^2 - K/W$)
NMMS	Non-Maximal Suppression	R_a	Rayleigh number
SML-HT	Sine Modulation Lamp Heating Thermography	S_k	k^{th} measuring area (m^2)
TAB	Using Analogies from coeval buildings	S_i	Material thickness
UAV	Unmanned Aerial Vehicle	S	Thickness of the material (m)
UND	University of North Dakota	T_s	Surface temperature (K)
Symbols	Definitions	T_p	Temperature of each pixel obtained from IR image (K)
Α	Area of the entire wall (summation of all A_i s) (m^2)	T_{sx}	Surface temperature at pixel x with bridges (K)
A_p	Area of each pixel in IR image (m^2)	T_{sxa}	Surface temperature at pixel x without bridges (K)
A_{ID}	Heat transfer area (m^2)	T_{ai}	Internal air temperature (K)
С	Specific Heat Constant	T_{ae}	External air temperature (K)
d	Specimen thickness	T_{si}	Internal surface temperature (K)
d_k	Thickness (m)	T_{refl}	Reflected surface temperature of area A_i (K)
F_j	View factor constant	T_m	Mean temperature (K)
h_i	Internal Convective Coefficient	t_D	Thermal diffusivity (m2=s)
h_e	External Convective Coefficient	U	Thermal transmittance coefficient $W/(m^2 - K)$
h_{si}	Internal surface heat transfer coefficient $(W/(m^2K))$	w	Water Content present in the element (%)
h_{ID}	Heat transfer coefficient	α_c	Convective heat loss coefficient
h_{se}	External surface heat transfer coefficient $(W/(m^2K))$	α_r	Radiative Heat loss coefficient
h_{cx} h_{cxa}	Convective with thermal bridges Convective without thermal bridges	ε γ	Emissivity Dry density (g/cm^3)
h_{rx}	Radiative coefficient with thermal bridges	λ_k	Thermal conductivity for k^{th} layer
h_{rxa}	Radiative coefficient without thermal bridges	φ	Heat flow(W)
h_i	Internal convective heat transfer coefficient	Ψ	Thermal bridge heat flow rate per unit temperature difference $(W/m - K)$
h_e	External heat transfer coefficient	ρ	Density (m ⁻ 3)
h_{ce}	External convective heat transfer coefficient	σ	Stefan-Boltzmann constant
l_{tb} l_{x}	Incidence factor of Thermal Bridge Pixel length with thermal bridge(m)	τ	Duration of heat loss (s)

amount of resistance provided by the building element for a specific thickness to the overall heat flow. Section 3 details different quantitative indices (U, Q, R, λ, I) used for various building elements.

These assessment methods, however, are susceptible to external environmental conditions and measurement errors may occur due to factors such as: (1) surface properties like emissivity, roughness, reflexivity, stains, and colors; (2) environmental factors such as incident solar irradiance, cloud presence, humidity, ambient temperature, moisture, and wind speed; and (3) miscellaneous factors that include distance, field of view, building orientation, and presence of unwanted objects (e.g. trees, ground, and sky) [4–9]. Measurement errors, however, can be minimized by adopting recommendations from standards such as ISO Directive 2012/27/UE [10,11], CEN [E-1213] [12], and ASTM (E-1543) [13–17]. Their recommendations include (1) positioning of camera perpendicular to the building; (2) wind speed must be

less than 5 m/s [18,19]; (3) temperature difference between the internal and external wall surface should be at least 10° C; and (4) the inspected surface must ideally be free from any solar radiation. Thus, aerial inspections using UAVs equipped with an IR camera can be considered as a suitable approach to perform thermal assessments of buildings.

There are limited existing comprehensive surveys available for the qualitative and quantitative heat-loss estimation techniques. Our extensive state-of-the-art literature review show that the availability of affordable light-weight IR cameras and UAVs can revolutionize the process of thermal assessment for buildings. Thermal assessment for small and medium-sized buildings using IR-based aerial thermography is a relatively straightforward process compared to high-rise buildings [20]. Moreover, IR-mounted UAVs consume less time and cost and can be stretched to hard-to-reach areas (e.g., roofs and underground structures). For this paper, we analyze medium-sized buildings with building

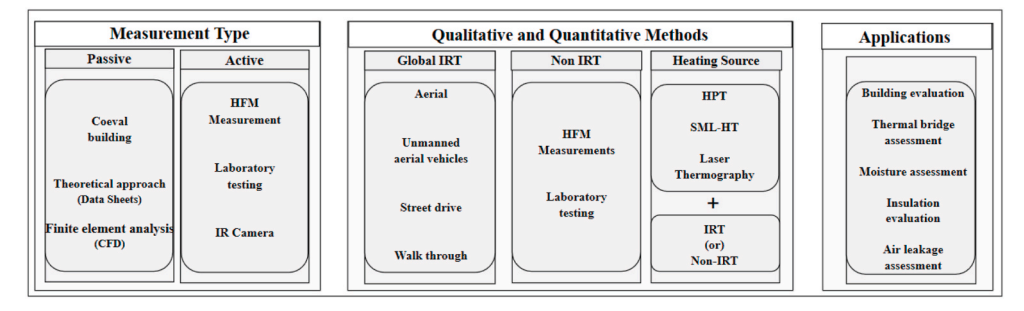


Fig. 1. Classification of thermal performance assessment of buildings.

Table 2Summary of qualitative measurements.

Measurement Scope	Details of Data	Sensors	Methodology	Comments	Reference
	Collection	and Accessories	-		
Outdoor Qualitative M	leasurements				
Building structure surveillance using an IR camera for possible degradation	IR camera was used to capture thermal images of outdoor building structures	IR camera	Non-Destructive Testing (NDT) method used for assessment of physio-chemical treatments such as stone cleaning, consolidation in historical structures and buildings	- No validation or sensitivity analysis	2002 [37], 2003 [38]
Detection of moisture in various buildings using an IR camera	IR camera was used to capture thermal images for a duration of 600 h Thermocouples were used to validate the results	IR camera, thermometer, thermocouples	Moisture detection was carried out using an IR camera thermometer and thermocouples under different conditions while varying time, distance and view angle	+ Validation shows 2.5-8.5% deviation from actual measurements + Sensitivity analysis for moisture detection was also carriedout	2016 [39] 2013 [40]
Detection of building thermal bridge using an IR camera	122 residential buildings in South West England were inspected for a duration of one month using IR cameras	IR camera	Pass by thermography: where an IR camera is mounted on top of a car to capture pass-by thermal images of building faces	+ Pass-by thermography is less expensive compared to walk- by thermography - No validation	2004 [41] 2016 [42]
Detection of air leakage for various buildings using IR cameras	IR camera was used to capture thermal images for a duration of 2 months	IR camera, temperature & humidity sensor, weather station	IR camera is used to detect air leakage through the roller shutter handle and the window frame of a room Portable fans were used to generate temporary pressure difference	+ Sensitivity analysis for varying pressure difference was carried out - No validation	2017 [43] 2013 [44]
Indoor Qualitative Me					
Assessment of thermal performance using an IR camera	Thermal images were catured using an IR camera	IR camera	NDT method was used for thermal performance assessment	+ Emissivity correction was carried out - Verification of the measurements was not provided	2016 [45]
Detection of hidden cracks using an IR camera in a laboratory environment	EasyHeat 224 Ambrell induction heater system used for coil excitation. SAT-HY6850 thermal camera used to record the thermal responses of the specimen for the duration of 2.4 s	IR camera, heater	Eddy current pulsed thermography: heat is generated using heater system and thermal camera captures the anomaly to detect the hidden cracks	- No validation	2016 [46]

area ranging from 30,000 to 50,000 sq. ft.

This paper contributes to the following specific aims:

- A comprehensive review and classification of thermal measurement techniques based on type, method, application, and quantification indices.
- A novel data-driven, three-layered (database, pre-processing and automation, and evaluation) framework for estimation of heat-loss using UAS-based thermal imagery.
- Machine learning based techniques (Mask R-CNN) to detect and segment building elements and to accurately quantify the heat-loss (or U-value) by processing thermal images (~5000 thermal images were captured on the UND campus).

The remainder of the paper is organized as follows: Section 2 provides a broader classification of qualitative or quantitative thermal performance measurement techniques and their applications with an exhaustive literature review; Section 3 classifies these measurement techniques based on the various quantification indices used for heat-loss estimation; Section 4 introduces a three-layered data-driven framework

for UAS-assisted thermal-imagery based heat loss quantification; Section 5 discusses results for the proposed machine learning model and heat-loss evaluation; and Sections 6, 7, and 8 end with a conclusion, pointers for future work, and acknowledgment respectively. Table 1 lists the nomenclature used throughtout the paper.

2. Classification of thermal performance measurement techniques based on measurement type, method, and applications

This section reviews several measurement techniques that are currently available to assess thermal performance of building envelopes with specific emphasis placed on the measurement type, methods, and applications as shown in Fig. 1. Some of the case studies on assessment of overall thermal performance of buildings, detection of thermal bridges, moisture, and air leakage are discussed in detail (Table 2). The objective of this section is to provide a literature survey and discover the appropriate technique (over various parameters such as ease of deployment, cost effectiveness, time consumed, detection capability, environmental effects, and attainability) that exists in the literature to











Fig. 2. Infrared thermal imagery: (a) aerial inspection using an Airbus plane [47]; (b) aerial inspection using an Airbus helicopter [48]; (c) automated fly inspection using UAVs [49]; (d) street drive inspection using vehicle [50]; (e) hand-held IR camera used for general walk through inspection [51].

analyze the thermal performance of campus buildings.

2.1. Measurement type

The thermal performance assessment techniques can be either passive or active type. Passive measurements are carried out by using data sheets or using similar buildings. On the other hand, in active measurements, variables like wall surface temperature, inside or outside air surface temperature, wind velocity, etc. are measured.

2.1.1. Passive measurements

Passive measurements can further be divided into coeval buildings, theoretical approaches, and finite element analysis. In coeval buildings, thermal assessment is done for structures of similar age, geographical location, and material compositions [21–24]. This technique is applicable when the actual building measurement is not possible. However, this method is often challenging due to missing building information such as construction periods, material compositions, and wall thickness and texture [25–30]. In theoretical methods [31–33], the R-value (or U-value) of buildings is calculated from the thermal conductivity and thickness of individual layers of a wall [34]. Simulation based design for 3D building envelopes is considered in finite element analysis method [35,36].

2.1.2. Active measurements

Active measurement techniques can be classified into HFM based measurement, laboratory testing, and IR thermal imaging.

2.1.2.1. HFM measurements. In this test, heat flow of the inspected element is measured using a Heat-Flux Meter (HFM) which consists of thermistors, transducers, a heat-flux plate (or heat flux sensor), and a data-logger [52–59]. The measurement accuracy depends on the type of instruments, installation procedure, data-capturing, and calibration mechanisms which includes position of the measurement apparatus, non-homogeneity of the materials, and the amount of water or moisture present in the material [60–66]. It is highlighted that solar radiation can interfere with HFM measurements. Hence, the measurements were carried out during dawn or dusk [64–66]. If the heat flow between the interior and exterior is low or the temperature difference is lower than 10° C, then measurements taken may not be accurate [64–66].

Laboratory Testing. In laboratory testing, the thermal performance

of a wall specimen is evaluated in a controlled lab environment [67–70]. In this environment, HFM or Guarded Hot Plate (GHP) based lab equipment is used to measure the thermal performance according to the International Standard ISO 8301 [64–66]. The measured heat flow rate from GHP combined with temperature difference are used to estimate the U-value [69,71,71–80].

IR thermal imaging. In IR thermal imaging, the thermal performance of a grey body is typically quantified using indices such as the U-value, R-value, etc. [10-17,81,82]. These indices can evaluate structural properties such as thermal bridges, emissivity of building facades, roofs, windows, and glazing systems.

The advantages of using an IR camera include nondestructive measurement, coverage of a larger inspection area in limited time, immediate access to raw surface temperature data, and acquisition of continuous imagery that can be logged remotely. However, environmental factors such as humidity, wind speed, air temperature, and solar radiation can limit the accuracy in estimating the surface temperature [83]

2.2. Qualitative and quantitative methods

The measurement techniques can be divided into qualitative or quantitative. Qualitative measurements are helpful in evaluating the overall thermal performance of buildings by identifying locations of maximum heat loss and/or possible thermal bridges, or assessing the quality of the thermal insulation, without quantifying the thermal loss [84,85]. A summary of various indoor and outdoor qualitative measurements are given in Table 2. Table 2 denotes the details of data-collection, measurement type, and methodology. The "Comments" column shows positive (+) and negative (-) aspects for each method. These methods are effective due to their lesser processing times, costs and efforts [86]. Uneven thermal patterns created by moisture or dampness can also be detected using qualitative measurements. The water content hidden in the wall acts as storage of additional heat and affects the overall thermal performance. The effect of air leakage can also be detected using qualitative thermal measurements.

The most cited heat loss coefficient in literature is the U-value, and it is defined as the rate of heat flow across one square meter of a surface when there is a temperature difference of one Kelvin [87] between the inside and outside surfaces (or vice-versa) and is expressed in W/m^2K . Hence, we adopted U-value as the quantitative metric to estimate the

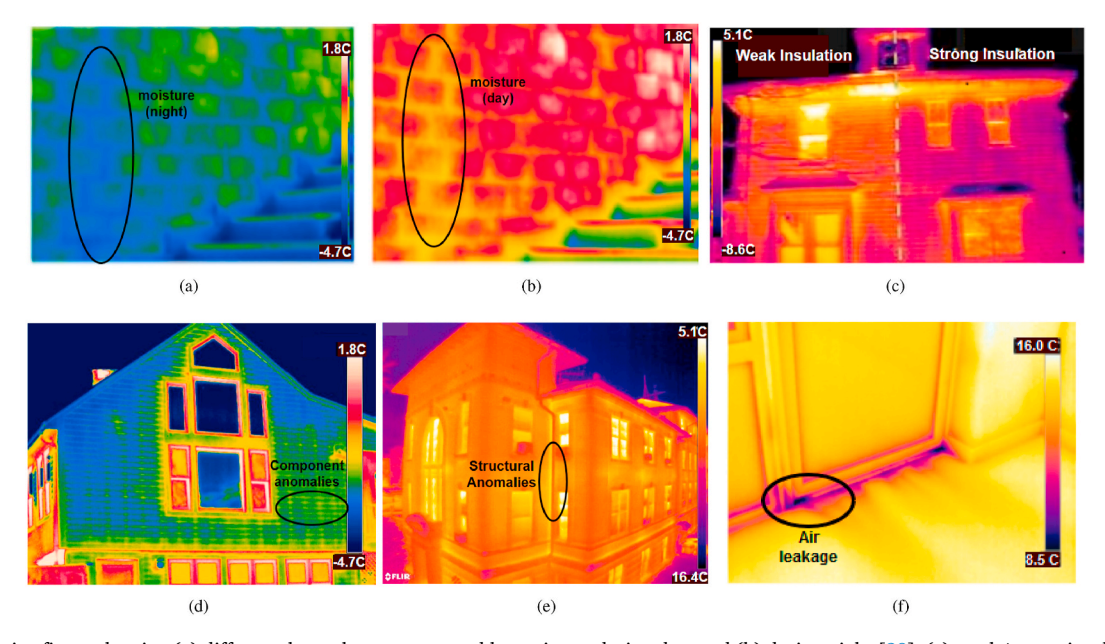


Fig. 3. Comparative figure showing (a) different thermal patterns caused by moisture during day, and (b) during night [39]; (c) weak/strong insulation of building wall [94]; (d) component anomalies: frame within wall is visible [95,96]; (e) structural anomalies detected near windows, junctions between two external walls, and pillar joints [97]; and (f) air leakage detected from thermal images [44].

heat-loss for our UAV based building data sets (e.g., Twamley and Museum).

Based on the type of apparatus used, the qualitative and quantitative assessment techniques can be further categorized into global IRT, non-IRT, and heating source based evaluation.

2.2.1. Global IRT

In this technique, IR thermography is used to evaluate the overall thermal performance of the entire building (mostly outdoor environments). Hence, these techniques are susceptible to the external environmental conditions. These techniques can be divided into aerial inspection, unmanned aerial vehicle inspection, street drive inspection, and walk through inspection (see Fig. 2).

Aerial inspections [40,88] (see Fig. 2) refer to the use of IR cameras installed on an airplane or a helicopter. Automated fly inspection measurements use an IR camera mounted on an (automated) UAV (see Fig. 2) without human interventions. These techniques suffer from licensing restrictions, higher equipment costs and drone vibrations [88]. Thermal images are captured using an IR camera mounted on a vehicle which runs through various streets or roads in street drive inspection [42,88,89]. MIT (Massachusetts Institute of Technology) developed a system called the "kinetic super resolution process" that can capture high resolution thermal images using a slow driving vehicle which is more cost effective than walk through inspection [42,90]. In walk through inspection (see Fig. 2), a thorough scan of different faces has been carried out by walking around the building with a hand-held IR camera [86]. This technique is also applicable for internal thermal performance assessment, however it consumes more time and effort. In addition, the thermal videos can capture possible temporal effects [91–93]. In general, the IRT techniques require uninterrupted power and can be impacted by the presence of obstacles. Moreover, the external approaches are susceptible to environmental conditions [85].

However, in these methods, measurement errors may occur due to different reasons such as: (1) surface properties like emissivity, roughness, reflexivity, stains, and colors; (2) environmental factors such as incident solar irradiance, cloud presence, humidity, ambient temperature, moisture, and wind speed; and (3) miscellaneous factors that include distance, field of view, building orientation, and presence of unwanted objects (e.g. trees, ground, and sky) [4–9].

The measurement errors, however, can be minimized by adopting standards such as ISO Directive 2012/27/UE [10,11], CEN [E-1213] [12], and ASTM (E-1543) [13-17]. Their recommendations include (1) positioning of camera perpendicular to the building; (2) wind speed must be less than 5 m/s [18,19]; (3) temperature difference between the internal and external wall surface should be at least $10^{\circ}C$; and (4) the inspected surface must ideally be free from any solar radiation. Thus, aerial inspections using UAVs equipped with an IR camera can be considered as a viable option for thermal assessments of buildings.

2.2.2. Non-IRT

The non-IRT based methods can be divided into HFM based techniques and laboratory testing whereas in laboratory measurements, the thermal performance of a wall specimen is evaluated in a controlled lab environment using HFM or Guarded Hot Plate (GHP) based lab equipment [67–70].

2.2.3. Heating source

Sometimes, heating sources are used in combination with IRT or non-IRT measurements. One or more heating sources is used to heat the surface of a test specimen in order to capture the thermal anomaly in the transient phase. The thermal anomalies, like hidden cracks or moisture, can be captured using an IR camera or an HFM in the presence of a heater. Based on the type of heating source, these techniques can be categorized as Heating Pulse Thermography (HPT), Sine Modulated Lamp Heating Thermography (SML-HT), and laser thermography.

In HPT, a pulse of short duration from a heater is applied on the inspected object. The temperature variation during transient states of heating and cooling is recorded using an IR camera [99]. An alternative heating source based on eddy current is used in Ref. [46]. In SML-HT, heat is applied periodically using a sine modulated lamp to produce the temperature variations [4,5]. In laser thermography, the laser beams are used as a heating source [6,7].

2.3. Applications

Based on the applications, different thermal measurement techniques can be used for overall building evaluation, thermal bridge assessment, moisture detection, assessment of insulation, and

Table 3Characteristic review of qualitative and quantitative IRT and non-IRT techniques.

	1							
	Technique							
Characteristics	HFM based techniques	Pulsed thermography	GHP based techniques	Lock-in thermography	Aerial/ UAV -assisted IRT	Laser spot thermography	Street-drive inspection	Walk-through inspection
Ease of deployment	Low	Low	Low	Moderate	High	Low	High	High
Cost effectiveness	Low	Low	Low	Low	High	Low	High	Moderate
Time consumed	High	Moderate	High	High	Low	High	Low	Moderate
Non-destructive	No	Yes	No	Yes	Yes	Yes	Yes	Yes
Surface anomaly detection	Yes	Yes	Yes	Yes	Yes	Yes	Yes	Yes
Hidden anomaly detection	No	Yes	No	Yes	No	No	No	No
Environmental effects	Low	Moderate	Low	Moderate	High	Moderate	High	High
Vibration	Low	Low	Low	Low	High	Low	Moderate	Low
External heating source	No	Yes	No	Yes	No	Yes	No	No
IR camera	No	Yes	No	Yes	Yes	Yes	Yes	Yes
Building survey	No	No	No	Yes (limited)	Yes	Yes (limited)	Yes (limited)	Yes
Roof inspection	No	No	No	No	Yes	No	No	Yes
Wall Inspection	Yes	Yes	Yes	Yes	Yes	Yes	Yes	Yes
Window/Door Inspection	No	No	No	Yes (limited)	Yes	Yes (limited)	Yes (limited)	Yes
Туре	QN	QN & QL	QN	QN & QL	QN & QL	QN & QL	QN & QL	QN & QL
References	[52–59]	[46,98]	[67–70]	[7]				[42,90]

assessment of air leakage (Fig. 3).

2.3.1. Assessment of overall thermal performance

The thermal performance evaluation helps in assessing the overall thermal conductivity (ability of a specific material to conduct heat), heat capacity, thermal emissivity (effectiveness in emitting energy as thermal radiation), thermal diffusivity (temperature spread through the surface), and material density of buildings [86]. These measurements can be carried out for shorter or longer duration.

The short term measurements need to comply with the international standards developed by International Standard Organization (ISO) [10, 11], European Committee for Standardization (CEN) [12], and American Society for Testing and Material (ASTM) [13–17]). Short time measurements are generally conducted from few hours to several months and are useful in evaluating various properties of the wall, like age [38,100], constituent materials [30,37,101], thickness [84,102], geometry [30,44,45], surface properties of the wall [30], and sub-components and their alignment within the wall [86].

The long term measurements are valuable in providing deeper insights into the progression of the thermal anomalies, and these measurements typically continue for several years [103–105]. The building degeneration assessment due to the presence of moisture over a period of several years is an example of a long-term measurement technique [106,107].

2.3.2. Detection of thermal bridges

Thermal bridges are defined as an area having a higher thermal conductivity than the surrounding areas, thereby providing less resistance to heat transfer. The two types of thermal bridges are structural and component. The structural bridge is formed by the building structures such as junctions and connections between two external walls, roof or floor joints, window joints, pillar joints, etc. (see Fig. 3). The component bridge, as shown in Fig. 3, is created by the abnormalities present in the materials or the problems associated with alignment of various components such as timber stud, steel wall ties, etc. [18,34,44, 108–112].

2.3.3. Detection of moisture and water content

Moisture, dampness or water content on walls can result in

evaporative cooling and can create uneven thermal patterns which can be detected by an IR camera [34,39]. The moisture or dampness detection can help in corrective measures for increasing the lifetime of buildings and removing the chances of any biological bacterial growth.

The best time to detect any possible water trace in the outside wall is in the early evening after a sunny day. As the solar radiation aids the evaporation process, the water traces can be easily captured using IR cameras [34] (see Fig. 3). In Ref. [113], laboratory experiments are carried out for moisture detection using additional cooling and heating system. Thermal performance assessment techniques can identify the water traces. However, these methods have limitations with respect to specific environmental conditions. Additional tools such as moisture meter and calcium carbide sampling can be used to increase the detection accuracy [39,113].

2.3.4. Assessment of thermal insulation

Qualitative and quantitative measurements are effective for the assessment of an insulation system. Specifically, these measurements can be used to detect absence of the insulation materials [34,41,85,114], non-working or damaged insulation components [34,84,114,115], and misaligned insulation components [34] (see Fig. 3). Damage of the insulation is caused by the detachment, shrinkage, low adhesion [44], and cracking of board panels, and finishing systems abnormalities [116]. In order to capture these defects, the standard procedures include maintaining a temperature difference of at least 10°C between the internal and external wall for at least 4 h before assessment [116].

2.3.5. Detection of air leakage

Air leakage affecting the overall temperature gradient of the wall surface can be captured using IR cameras (see Fig. 3) [44,117,118]. The impact of air leakage on the temperature gradient increases with the magnitude and size of the leakage [34,43]. The air leakage can be detected successfully if the temperature and pressure difference between inside and outside building (or wall) is at least 10°C and 10 Pascals, respectively [43,44]. Generally, a mechanical device like a fan or ventilation system is used to create an artificial pressure difference [119, 120]

A detailed comparison of various quantitative approaches used for indoor and outdoor measurements is given in Tables 4-6 respectively.

Journal of Building Engineering 32 (2020) 101637

Table 4
Summary of quantitative outdoor measurements.

Author	Year	Building element analyzed	Equipment used for measurement	Measurement duration	Validation	% Error	T_{refl} compensation	arepsilon-measurement	Sensitivity analysis	Comments
Quantification I	ndex - He	at Transfer Coeff	icient (U)							
Albatici et al. [63]	2008	Wall surface	IR camera, anemometer, heater	NA	CAL	32	NA	Y	NA	- No sensitivity analysis
Albatici et al. [121]	2010	Wall surface	IR camera, soldering iron, anemometer	NA	CAL MEAS	30–161 53	NA	Y	NA	+ Accurate results obtained by avoiding solar radiation, with 10K temperature difference & minimum wind velocity
Taylor et al. [44]	2013	Building	HFM, thermometer	7-14 days	CAL	2–154	NA	NA	NA	+ On-site assessment during building construction for preventive analysis
Dall et al. [122]	2013	Building	IR camera	NA	CAL	2–154	Y	Y	NA	+ Used for energy audit application
Nardi et al. [123]	2014	Building	IR camera, hosespipe	24 days	CAL MEAS	29 38	NA	NA	NA	+ IRT results are verified using theoretical and HFM measurements - No sensitivity analysis
Nardi et al. [124]	2015	Wall surface	IR camera, hosepipe	NA	CAL MEAS	46 47	Y	Y	NA	 + Different thermal mass of walls considered - No sensitivity analysis
Albatici et al. [125]	2015	Wall surface	IR camera, weather station, thermohygrometer	1 h	CAL MEAS	23 22	NA	NA	Y	+ IRT results were validated using HFM measurement - Sensitivity analysis showed IRT estimation deviates by 9%, 27%, and 50% when the wind, inner and outer temperature deviate by 9% respectively
Choi et al.	2017	Wall surface	IR camera, anemometer	NA	CAL MEAS	1–44 5–42	Y	Y	Y	+ Sensitivity analysis, + Reflected temperature compensated
Madding et al. [126]	2008	ermal Resistance Wall surface	IR camera, weather station	24 h	MEAS	12	Y	NA	Y	+ Temperature difference is highlighted as most influential
Ham et al. [127]	2014	Building	IR camera, optical camera, thermometer	NA	NA	NA	NA	NA	NA	+ Building 3D model was constructed using thermal and digital imagery
Ibos et al. [128]	2015	Wall surface	IR camera, weather station, thermocouples, emissometer	3-7 days	CAL MEAS	57 60	NA	Y	NA	+ Emissivity measured using emissometer - No sensitivity analysis
Marino et al. [87] Quantification I	2017 ndex - To	Building	IR camera, laser distance meter, thermometer, thermo-resistances, weather station	4 days	NA	NA	Y	Y	NA	+ Evolution of spatial thermal resistance was shown
Ghiaus et al. [129]	2006	Building	NA (using weather data and building energy consumption model)	1 month	NA	NA	NA	NA	NA	+ Regression based model from weather data
Vavilov et al. [115]	2010	Wall surface	IR camera, heat gauge sensor, temperature sensor	236 days	CAL MEAS	3–193 10	NA	NA	NA	+ Validated using HFM measurement
Vollaro et al. [130]	2015	Building	IR camera (and building data sheet)	8640 h	MEAS	12–14	NA	NA	NA	+ Results obtained from data sheet are validated using HFM measurements and an IR camera
Quantification I	ndex - Tei	nperature Distril	oution Coefficient (T_d)							
Kim et al. [131]	2016	Building	IR camera	12 months	NA	NA	NA	NA	NA	 No validation or sensitivity analysis performed

These tables provide a summary of the scope of measurement, data collection process, errors, sensor type, quantification indices, advantages and limitations, and relevant references in the literature review. In these studies, different measurement apparatus such as IR cameras, HFM, thermometers, thermocouples, and weather stations were used to estimate the temperature distribution, total heat loss, thermal transmittance, conductivity, and amount of thermal resistance of the building. In addition, actual measurements are carried out to aid in the credibility of these techniques.

The qualitative and quantitative heat-loss estimation techniques are compared in Table 3 The heat-flux meter based techniques are suitable for laboratory setup, but require additional instruments. Hence, these techniques requires more cost and time if deployed to conduct building heat loss survey. The HFM based techniques are effective for surface anomaly detection. The advantages of using such techniques are that they produce more accurate results and are not susceptible to environmental (or vibration) effects. Moreover, these techniques are applicable for quantitative surveys as they can estimate the heat-flux (Q) using HFM. Similarly, the GHP based techniques can estimate the heat-flux accurately at a cost of increasing time and efforts. The GHP based estimation uses a guarded heater and air-flow to measure the heat-flux in a controlled lab environment.

The Heating Pulsed Thermography (HPT) based techniques require additional instruments (such as heaters) to identify hidden anomalies (such as cracks) using an IR camera. The presence of an IR camera, heater and other instruments makes it difficult to conduct a building heat-loss survey. The HPT techniques can heat-up the inspected elements more quickly than HFM or GHP based techniques. The Lock-in Thermography (LT) based techniques apply a sine-modulated lamp heating over the inspected elements to produce a temperature difference. These methods are effective to identify hidden anomalies, and can be used to estimate the heat-loss of buildings, but requires additional setup. Laser spot thermography techniques use laser beams to generate external heat and can identify surface cracks. These techniques (HPT, LT, LST) can be applied to both qualitative and quantitative surveys.

The aerial or UAV/assisted IRT techniques are cost-effective and consume less time for set-up. These techniques help detect any presence of surface anomalies (e.g., cracks, leaks, or moisture levels) without the need for any external heating source. These techniques are also useful in conducting building surveys (including the roof). The street-drive IRT techniques are cheap compared to UAV-assisted IRT techniques, but trying to conduct full building surveys (especially the roof). Walk-through IRT techniques consume more time but are highly flexible. However, the UAV-assisted IRT techniques are easy to deploy, cost-effective, less time consuming, non-destructive, and can be extended for hard-to-reach areas. Hence, in this work, we utilize the UAV-assisted IRT technique for heat-loss assessment of the various campus buildings.

3. Heat-flow calculations, thermal conductivity, and resistance, and transmittance indices

This section details the process of heat-flow calculations focusing on thermal conductivity, temperature distribution, total heat loss, incidence factor of the thermal bridge, thermal resistance, and the thermal transmittance coefficient. The objective of this section is to investigate existing techniques for heat-loss quantification and emerge the best suitable quantification index for assessment of the campus buildings later in section 5.

3.1. Thermal conductivity

This index can be used to identify thermal anomalies like cracks, moisture, etc. The thermal conductivity (λ) can be measured using the thermal diffusivity (d_t) as given in the following equation [147]:

$$\lambda = \rho C d_t \tag{1}$$

where ρ and C denote the mass density and the specific heat constant, respectively. The thermal conductivity can be evaluated from the amount of heat flow [73] as given by

$$\lambda = \frac{\Phi d}{(T_{si} - T_{se})A} \tag{2}$$

where φ and d are the heat flow and specimen thickness, respectively, and are measured using laboratory equipment.

3.2. Temperature distribution coefficient

Hidden cracks can be identified using the temperature distribution coefficient. This method is applicable for homogeneous and isotropic materials. The spatial temperature distribution across the surface element for a 2D homogeneous surface must satisfy the following equality:

$$\frac{\partial^2 T}{\partial x^2} + \frac{\partial^2 T}{\partial y^2} = \frac{1}{d_t} \frac{\partial T}{\partial t}$$
 (3)

where T=T(x,y,t) denotes the surface temperature in x,y coordinates, and t denotes the time domain. The diffusivity constant can be given from Eq. (1). The cracks can be identified from those vicinity where Eq. (3) is not satisfied. The temperature difference can also be used for cracks and air leakage estimation [148,149].

3.3. Total heat flow measurements

The total heat loss, or heat flow, (*Q*) in a building element can be quantified using the following equation [115]:

$$Q = \sum_{k=1}^{N} Q_{cur\ k} \tau S_k \frac{T_{ur}^{in} - T_{uir}^{out}}{T_{in}^{in} - T_{uir}^{out}}$$
(4)

where $Q_{cur\ k}$ is the heat loss in the k^{th} zone (measured using a heat gauge sensor, see Fig. 4), τ is the duration of heat loss, N is the number of zones, and S_k is the k^{th} measuring area. An IR camera is used to capture the surface temperature T_s^{in} and the air temperature is measured using a thermometer. This method combines IR camera and heat gauge sensor technology. In Refs. [83], the Q-value is quantified as:

$$Q = \varepsilon \sigma \left(T_{hot}^4 - T_{cold}^4\right) + \alpha_c \left(T_{hot} - T_{cold}\right) \tag{5}$$

where T_{hot} and T_{cold} denote the temperature of hot and cold sides of the wall, respectively. The density of heat flow rate (which is heat flow rate per unit area, Wm^{-2}) is used as the quantification index in Ref. [136] and it is given by

$$q_{density} = q_r + q_c \tag{6}$$

where $q_r=q_{o.s}-q_{i.s}$. $q_{o.s}$ and $q_{i.s}$ denote the outgoing heat flow rate and incoming heat flow rate (per unit area), respectively, and they are expressed as

$$q_{o,s} = \varepsilon \sigma T_s^4 + (1 - \varepsilon) q_{i,s} \tag{7}$$

$$q_{i,s} = \sum_{i} F_j q_{o,s,j} \tag{8}$$

where F_j is a constant and $q_{os,j}$ is the outgoing heat flow rate per unit area for the surface j.

3.4. Incidence factor of thermal bridge (I_{tb})

This index evaluates the performance of a building element by comparing it with an ideally insulated building material. It is used to quantify the performance of a thermal bridge and can be given as the

Journal of Building Engineering 32 (2020) 101637

 Table 5

 Summary of quantitative indoor measurements (part I).

Author	Year	Building element analyzed	Equipment used for measurement	Measurement duration	Validation	% Error	T_{refl} compensation	arepsilon-measurement	Sensitivity analysis	Comments
Quantification Ind	ex - Heat	Transfer Coefficie	ent (U)							
Kato et al. [132]	2007	Wall surface specimen	IR camera	5 days	MEAS	6	NA	NA	NA	+ Validated using HFM measurements- No sensitivity analysis
Grinzato et al. [133]	2010	Wall surface	IR camera, anemometer	NA	CAL MEAS	8–114 8–95	NA	NA	NA	No sensitivity analysisNo emissivity correction
Fokaides et al. [33]	2011	Wall surface specimen	IR camera, thermohygrometer	3 h	CAL MEAS	59 21	NA	NA	Y	+ Validated using thermohygrometer and HFM + No sensitivity analysis
Thouvenel et al. [134]	2012	Wall surface	IR camera, thermocouple	10 h	CAL	5	NA	Y	NA	 + Emissivity correction provided - No sensitivity analysis
Ham et al. [135]	2013	Wall surface	IR camera	NA	NA	NA	NA	NA	NA	-No emissivity correction -No sensitivity analysis
Ohlsson et al. [136]	2014	Wall surface	IR camera, hosepipe, anemometer	1 h	MEAS	NA	NA	NA	NA	+Validated using HFM measurement - No emissivity correction - No sensitivity analysis
Simoes et al. [137]	2014	Wall surface specimen	IR camera, thermocouples, anemometer	1 h	MEAS	36	NA	NA	Y	+ HFM measurements used to validate results + Sensitivity analysis showed the effect of emissivity
Tzifa et al. [138]	2014	Wall surface specimen	IR camera, thermometer	24 h	CAL	2–204	Y	Y	NA	+ Emissivity correction was made using vinyl black tape, + Reflected temperature was considered + Validated using CAL method + Uncertainty quantification using U-value assessment
Nardi et al. [123]	2014	Wall surface specimen	IR camera	2 days	NA	NA	NA	NA	NA	- No sensitivity analysis
Nardi et al. [124]	2015	NA	IR camera, hosepipe, thermos-hygrometer	NA	CAL MEAS	7 13	NA	NA	NA	+ IRT measurements validated using HFM measurements - sensitivity analysis missing
Nardi et al. [139]	2016	Wall surface	IR camera, thermo-hygrometer, hosepipe	1 h	CAL MEAS	39 20	Y	Y	Y	+ Four different equations were compared + Sensitivity analysis and emissivity correction carried out
Donatelli et al. [98]	2016	Wall surface	IR camera, thermo-hygrometer, halogen lamps, anemometer	10 h	CAL	4	Y	Y	NA	 + Pulsed heating technique with halogen lamps was used + Emissivity correction - No sensitivity analysis
Tejedor et al. [140]	2017	Wall surface	IR Camera, thermo-hygrometer, thermocouple	2-3 h	TAB CAL MEAS	4 2–20 12–27	Y	Y	Y	+ Emissivity correction and sensitivity analysis were carried out
Marshall et al. [141]	2018	Wall surface	IR camera	NA	TAB MEAS	2–27 9	Y	Y	NA	+ Emissivity correction was carried out $+$ IR images with different resolution were captured

Journal of Building Engineering 32 (2020) 101637

 Table 6

 Summary of quantitative indoor measurements (part II).

			•							
Author	Year	Building element analyzed	Equipment used for measurement	Measurement duration	Validation	% Error	T_{refl} compensation	arepsilon-measurement	Sensitivity analysis	Comments
Quantification Inde	ex - Theri	nal Resistance (R)								
Kisilewikz et al. [142]	2010	Wall surface	IR camera, reflector, thermocouples	48 h	MEAS	43	Y	NA	NA	+ Emissivity measurements were carried out - Sensitivity analysis missing
Nardi et al. [143]	2014	Wall surface	IR camera	NA	MOD	73	NA	NA	NA	- Sensitivity analysis and emissivity correction were
W . 1 54007		11		0 = 1						missing
Ibos et al. [128]	2015	Wall surface	IR camera, weather station, thermocouples, emissometer	3-7 days	CAL MEAS	57 60	NA	Y	NA	+ Emissivity measured using emissometer - Sensitivity analysis missing,
Donatelli et al. [98]	2016	Wall surface specimen	IR-camera, thermo- hygrometer, halogen lamps, anemometer	13 h	CAL	4	NA	NA	Y	+ IR camera measurements were validated using HFM measurements + Sensitivity analysis was carried out
Quantification Inde	ex - Total	Heat Loss (Q)								
Danielski et al. [83]	2015	Wall surface specimen	IR-camera, thermometer	143 days	MEAS	11	NA	NA	NA	+ IRT measurements were validated using HFM measurements
Quantification Inde		0								
Asdrubali et al. [61]	2012	Doors, Windows	IR-camera, thermometer	NA	MEAS	5	NA	Y	NA	 No sensitivity analysis provided + Emissivity calibration carried out + Verified using measurements
O'grady et al. [144]	2017	Wall surface	IR-camera, anemometer	NA	MEAS	36	Y	Y	Y	+ Sensitivity analysis + Validated using HFM + Emissivity correction
O'grady et al. [145]	2017	Wall surface	IR-camera, anemometer	NA	MEAS	12	NA	NA	NA	- Sensitivity analysis, correction were missing + Validated using HFM
Baldinelli et al. [146]	2018	Wall surface	IR camera, temperature probes	NA	MEAS	52	Y	Y	NA	+ Emissivity correction carried out - Sensitivity analysis was missing
-		nal Conductivity (λ)								
Wang et al. [73]	2018	Wall surface	HFM, heating circuits, thermocouple	72 h	CAL MEAS	2–27 9	NA	NA	NA	 + Results were verified using theoretical methods - Sensitivity analysis missing

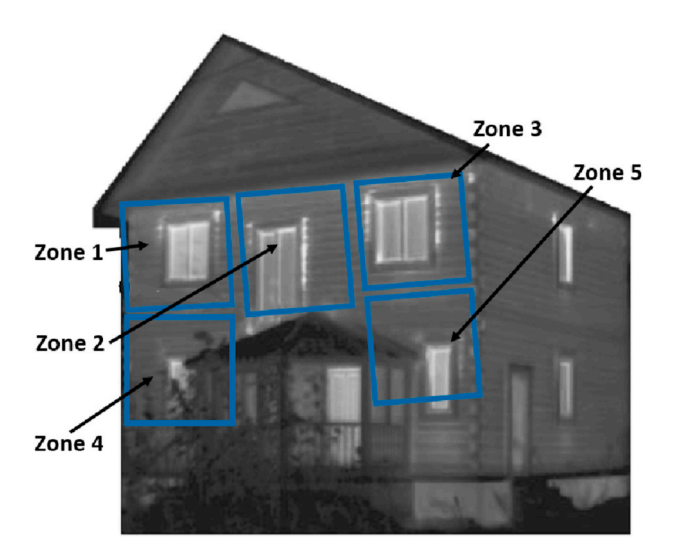


Fig. 4. The process of dividing the building into *K* zones [115].

ratio of heat flow with and without thermal bridges [61].

$$I_{tb} = \frac{Q_{tb}}{Q_{tD}} \tag{9}$$

where Q_{tb} and Q_{tD} denote the heat flow with and without thermal bridge, respectively, and can be expressed as

$$Q_{iD} = h_{ID}A_{ID}(T_{ai} - T_{si}) {10}$$

where $h_{\rm ID}$ and $A_{\rm ID}$, are the heat transfer coefficient and heat transfer area, respectively, and

$$Q_{ib} = h_{ib-i}A_p \sum_{p=1}^{N} T_i - T_p$$
 (11)

where h_{ID}, A_p, N , and T_p represent the heat transfer coefficient with thermal bridge, area of each pixel, number of pixels, and temperature of each pixel obtained from IR images, respectively. In Ref. [146], the incidence factor of thermal bridge, I_{tb} , is estimated as

$$I_{tb} = \frac{\sum_{x=1}^{N} (T_{ai} - T_{sx})}{N(T_{ai} - T_{sxa})}$$
 (12)

where N is the number of pixels.

In order to assess the overall performance of a thermal bridge, O'Grady et al. [144,145] investigated the thermal bridge heat flow rate per unit temperature difference (Ψ) which is expressed as

$$\Psi = \frac{q_{TB}}{T_{ci} - T_{ce}} \tag{13}$$

where q_{TB} denotes the thermal bridge heat flow rate, given by

$$q_{TB} = \sum_{\forall x} q_{xTB} \tag{14}$$

where q_{xTB} represents the thermal bridge heat flow rate for pixel x and it can be estimated as the difference between the heat flow rate of pixel x with (q_x) and without (q_{xa}) thermal bridges using the following expression:

$$q_{xTB} = q_x - q_{xa} \tag{15}$$

Here, q_x and q_{xq} can be expressed as,

$$q_x = l_x [(h_{cx} + h_{rx})|T_{ae} - T_{sx}|]$$
(16)

$$q_{xa} = l_{xa}[(h_{cxa} + h_{rxa})|T_{ae} - T_{sxa}|]$$
(17)

where l_x , l_{xa} , h_{cx} , h_{cxa} , h_{rx} , h_{rxa} , T_{sx} and T_{sxa} are pixel length with and without thermal bridges, convective and radiative coefficient with and without thermal bridges, and surface temperature at pixel x with and without bridges, respectively.

3.5. Thermal resistance

The thermal resistance or R-value is defined as the amount of resistance provided by the building element for a specific thickness to the overall heat flow. Therefore, when the R-value increases, the building element provides better insulation. The R-value is expressed in $m^2 - K/W$. This section provides details of various indices used to quantify the thermal resistance. The R-value can be estimated as the ratio of material thickness (s_i) to conductivity [150] (λ_i) as shown by

$$R = \frac{s_i}{\lambda} \tag{18}$$

Equation (18) shows the resistance for material *i*. If thermal conductivity and material thickness are not available, the resistivity can be estimated by

$$R = \frac{T_{ae} - T_{ai}}{4\varepsilon\sigma T_m^3 \left(T_{si} - T_{refl}\right) + \alpha_c \left(T_{si} - T_{ai}\right)}$$
(19)

[126,135]. The following equation is used to quantify the resistivity coefficient in Ref. [98],

Table 7Performance indices.

Performance Index	Duration	Building details	Indoor setup	Reference
	1920 h	NA	Indoor temp set at 25.2 C	[155]
	2190 h	Commercial hotel	25.5 C for summer, 20.5 C for winter	[156]
	5880 h (max)	40-storey building	25.5 C for cooling, 21 C for heating	[157-159]
OTTV	NA	40-storey building	25.5 C for cooling, 22 C for heating	[160]
	NA	Single compartment building	25 C	[161,162]
	34 yrs	39092 buildings	NA	[163]
	1 yr	1-storey building	NA	[164]
	1 yr	Multi-storey	NA	[165]
	1 yr	32-storey office building	Cooling: 26 °C,	[2]
	-		Heating: 20 °C	
PAL	1 yr	Multi-storey	NA	[165]
	1 yr	32-storey office building	Cooling: 26 °C,	[2]
	•		Heating: 20 °C	
OBEM	1 yr	Multi-storey	NA	[165]
ENVLOAD	1 yr	Multi-storey	NA	[165]
	NA	13-storey	NA	[166]

Table 8Guidelines to capture UAS-based thermal images.

Factor	Recommendation
Temperature difference	Internal and external wall temperature difference must be at least 10°C
Distance	Distance from IR camera to the wall surface should be atleast 5-15 m
Solar radiation	Avoid all source of solar radiation, preferable time for thermal image capturing is dawn or dusk
Angle	IR camera must be placed at an angle less than 60° to the surface
Wind speed	The wind speed must be less than 5 m/s between camera and inspected wall
Number of images	Atleast 40 images per position should be taken
Ambient temperature & humidity	Ambient temperature should ideally be below 35 $^{\circ}\text{C}$ and humidity below 80%

$$R = \frac{T_{ai} - T_{ao}}{5.67\varepsilon \left[\left(\frac{T_{wc}}{100} \right)^4 - \left(\frac{T_{out}}{100} \right)^4 \right] + \alpha_c (T_{wc} - T_{out})}$$
(20)

In multi-layer buildings, the resistivity can also be quantified as the summation of resistances in different layers as shown by

$$R = R_{si} + \frac{e}{k} + R_{se} \tag{21}$$

where R_{si} , R_{se} , s, and k denote the internal and external surface thermal resistances of the air boundary layers, thickness of the material, and proportionality constant (defined as the amount of heat that flows through a unit thickness of the material, $\frac{W}{m^2K}$, and can be retrieved from the material properties), respectively. In Ref. [65], the internal and external surface thermal resistances are replaced by the internal and external convective heat transfer coefficients, h_i , h_e , respectively, as

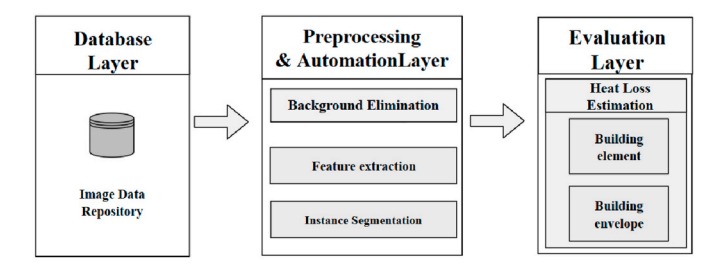


Fig. 6. Data-driven approach for thermal performance assessment.

follows:

$$R = \frac{1}{h_i} + \frac{e}{k} + \frac{1}{h_r} \tag{22}$$

3.6. Thermal transmittance coefficient

The thermal transmittance coefficient or the U-value of an internal wall surface is quantified in Ref. [132] as the ratio of total heat flow to the temperature difference:

$$U = \frac{\sum_{\forall i} \alpha_c (T_{ai} - T_{si}) + \alpha_r (T_{refl} - T_{si}) \times A_i}{(T_{ai} - T_{ae}) \times A}$$
(23)

where α_c and α_r respectively denote the convective and radiative heat loss coefficients, and T_{ai} , T_{ae} , T_{si} , and T_{refl} denote the internal air, external air, internal surface, and reflected surface temperature of area A_i , respectively. Moreover, A denotes the area of the entire wall which is the summation of all A_i s.

If the values for external heat transfer coefficient (h_{ce}) are available, the U-value of an external wall surface can be quantified using the

Table 9
Building datasets, window, and wall properties.

Building Name	Image Capturing details			Weather	Weather Details		Window property	Wall Properties			
	# images	Date	Time	Avg Temp (C)	Humidity (%)	Avg wind speed (mph)		Avg surface temp (thermocouple)	Emissivity	Surface type	Material type
	2480	9th Oct, 2019	06:30-07:30 h	NA	79	7		NA			Brick
Twamley Hall	878	17th Mar, 2020	07:00–20:00 h	21.2	69	10	Single pane glass	9.73	0.75	Rough	Brick
	906	8th Oct, 2019	18:55–19:55 h	18.0	55	9		14.9			Brick
Museum of Art	710	17th Mar, 2020	07:00–20:00 h	21.2	69	10	Double pane glass	2.56	0.75	Rough	Brick

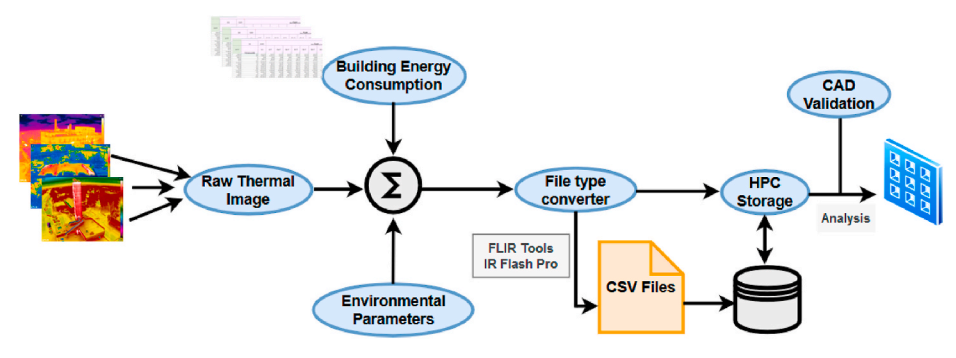


Fig. 5. Database layer.

 Table 10

 Comparison of accuracy of background elimination techniques.

Image #	False positives (%)	False negatives (%)	Total error (%)							
Canny Edge	Canny Edge Detection									
192	$\frac{370}{327680} = 0.11$	$\frac{44654}{327680} = 13.63$	$\frac{45024}{327680} = 13.74$							
118	$\frac{2}{327680} = 0.0$	$\frac{44654}{327680} = 33.61$	$\frac{45024}{327680} = 33.61$							
Dominant C	Color Isolation	027 000	02,000							
192	$\frac{13620}{327680} = 4.16$	$\frac{23555}{327680} = 7.19$	$\frac{37175}{327680} = 11.34$							
118	$\frac{2316}{327680} = 0.71$	$\frac{90030}{327680} = 27.48$	$\frac{92346}{327680} = 28.18$							

following equation [122,131]:

$$U = \frac{h_{ce} \times A_i \times (T_{ai} - T_{si})}{A \times (T_{ai} - T_{ae})}$$
(24)

According to Stefan-Boltzmann law, the radiative heat varies with the fourth power of temperature difference [151]. Madding et al. replaced the radiative coefficient α_r in Eq. (23) by $4\varepsilon\sigma T_m^3$ and introduced the following equation, which contains the radiative term according to the Stefan-Boltzmann law:

$$U = \frac{4\varepsilon\sigma T_m^3 (T_{si} - T_{refl}) + \alpha_c (T_{si} - T_{ai})}{T_{ai} - T_{ae}}$$
(25)

where $T_m = \frac{T_s + T_{refl}}{2}$, denotes the mean temperature. ε and σ denote the emissivity and Stefan-Boltzmann constant, respectively. Moreover, the reflective temperature is subtracted from the surface temperature in this equation. The emissivity constant was set between 0.95 and 1.00 [126]. The convective coefficient α_c depends on various factors, including the height of the wall and temperature difference, and is given by the following equation

$$\alpha_c = c_1 \frac{(T_{si} - T_{ai})_{\frac{1}{4}}}{L} \tag{26}$$

where L is the height of the wall and the value of c_1 varies from 1.31 to 1.42. A similar equation is used by Marshall et al. [141] where the mean temperature is replaced by surface temperature. Ham et al. have given

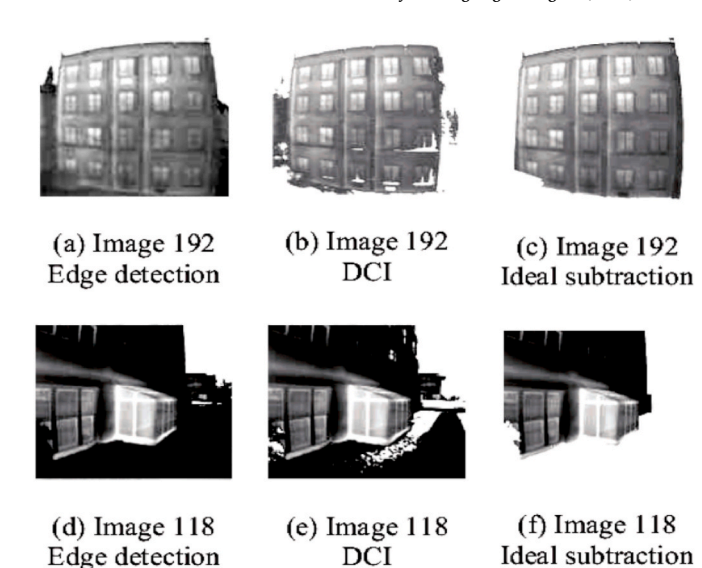


Fig. 8. Comparison of various methods.

similar equation in Ref. [127,134,135], where fourth power of reflected temperature is subtracted from fourth power of surface temperature as given by

$$U = \frac{4\varepsilon\sigma\left(T_s^4 - T_{refl}^4\right) + \alpha_c(T_s - T_{ai})}{T_{ai} - T_{ae}}$$
(27)

where T_s denotes the surface temperature.

Tzifa et al. [138] suggested that if the reflected temperature is not available, it can be replaced by the air temperature in Eq. (27). The internal (α_{ci}) and external (α_{ce}) convective coefficients are considered to estimate the U-value in Ref. [98] as given by

$$U = \frac{1}{\frac{1}{a_{ci}} + \frac{T_{ai} - T_{ae}}{4\epsilon\sigma \left(T_s^4 - T_{eig}^4\right) + a_c (T_s - T_{ai})} + \frac{1}{a_{ce}}}$$
(28)

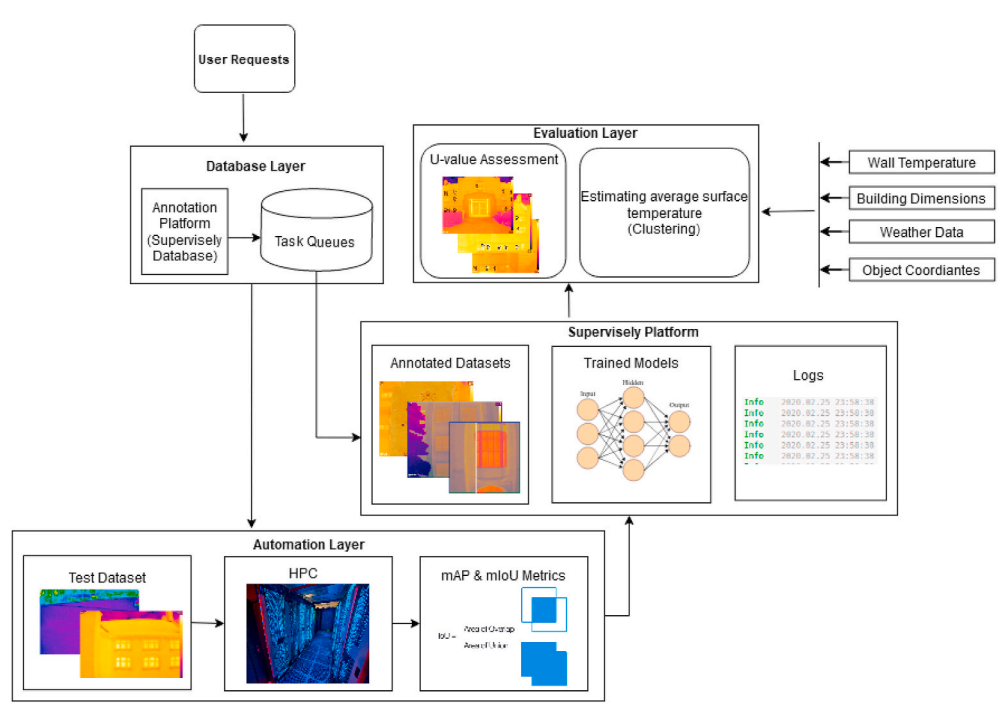


Fig. 7. Machine learning workflow for U-value estimation.

Table 11Mask R-CNN model training parameters.

Model Name	Learning Rate	Input Resolution	Number of GPU's	Epochs
	0.00001	256X256	1	200
	0.00001	256X256	1	5
	0.00001	256X256	1	200
	0.00001	256X256	1	100
	0.00001	256X256	1	100
	0.00001	256X256	1	50
	0.00001	256X256	1	100
	0.0001	256X256	1	10
	0.0001	256X256	1	10
Mask RCNN	0.001	256X256	1	50

Table 12Mask R–CNN evaluation metrics.

Object	AP ^{0.25}	AP ^{0.50}	AP ^{0.75}	IoU
Window	0.68	0.67	0.37	0.05
Façade	0.58	0.46	0.27	0.50
Average	0.63	0.56	0.32	0.46

In order to determine the convective heat transfer coefficient α_c , the Rayleigh number R_a , Prandtl number P_r , height of the wall L, and the thermal conductivity of the fluid k_c , are used in Ref. [140] as follows,

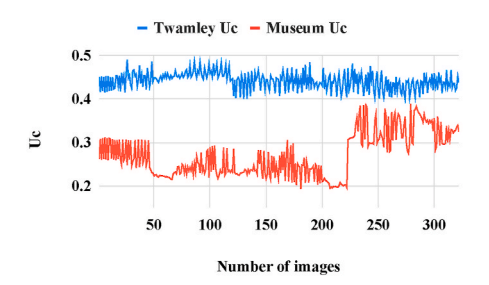
$$E\sigma\left(T_{refl}^{4} - T_{si}^{4}\right) + \frac{k_{c}}{L}\left(0.825 + 0.325R_{a}^{\frac{1}{b}}\right)^{2} (T_{ai} - T_{si})$$

$$U = \frac{T_{ai} - T_{ae}}{T_{ae}}$$
(29)

If the fluid is air, then the value of k_c is 0.025 $Wm^{-1}K^{-1}$ when the temperature is between 20°C to 25°C. The U-value estimation for the external surface is carried out using the following equation, where the wind velocity is considered [125,139,152]

$$U = \frac{\varepsilon\sigma(T_{se}^4 - T_{ae}^4) + 3.805\nu(T_{se} - T_{ae})}{T_{ai} - T_{ae}}.$$
 (30)

where v is the velocity of external wind. The radiative heat component is similar to Stefan-Boltzmann equation [151] and the convective term is derived from Jargon's formulae [153]. If HFM is available, the estimation of U-value is straight forward and can be done as follows [122].



(a) Single vs double pane window average U_c analysis

$$U = \frac{\Delta Q}{t_{ac} - t_{ai}} \tag{31}$$

where Q is estimated using an HFM. The U-value can also be estimated from the thickness and thermal conductivity [154] as given below.

$$U = \frac{1}{\frac{1}{h_{cl}} + \frac{1}{h_{cs}} + \sum_{k=1}^{n} \frac{d_k}{\lambda_k}}$$
 (32)

Here, d_k is the thickness, and λ_k is the thermal conductivity for each layer, and h_{si} and h_{se} are internal and external surface heat transfer coefficients, respectively.

3.7. Performance indices

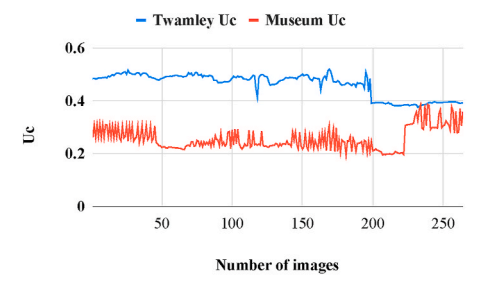
Performance indices (such as Overall Thermal Transfer Value (OTTV), Envload index, Perimeter Annual Load (PAL), Office Building envelope Energy performance and configuration Model (OBEM) index) of a building, as listed in Table 7, show the overall thermal (or heat loss) performance and provide architects valuable insights for innovative building designs [167]. The American Society of Heating, Refrigerating, and Air Conditioning Engineers (ASHRAE) defines the OTTV as a measure of average heat transfer into the building over its building envelope [168,169]. This metric was first introduced by ASHRAE in Standard 90-75 [169] and is defined as "the maximum thermal transfer permissible into the building through its walls or roof, due to solar heat gain and outdoor–indoor temperature difference". The OTTV can be estimated for external walls and for roofs by using the two equations as follow

$$OTTV_{W} = (U_{w} \times A_{w} \times TD_{EQ}) + (A_{f} \times SF \times SC) + (U_{f} \times A_{f} \times \Delta T))$$
(33)

$$OTTV_R = ((U_R \times A_R \times TD_{EQ}) + (434.7 \times A_S \times SC) + (U_S \times A_S \times \Delta T))$$
 (34)

where $OTTV_W$ and $OTTV_R$ respectively denotes the OTTV of an opaque part of wall and roof (in W/m2); U_W , U_f , U_R , and U_S denote the thermal transmittance of opaque part of wall, fenestration, opaque part of roof, and skylight, respectively (in W/m^2-C ; A_W,A_f,A_R and A_S respectively denotes the area of the opaque part of a wall, a fenestration, the opaque part of a roof and a skylight, respectively (in m^2); TD_{EQ} denotes the (inside and outside) temperature difference for the opaque part of a wall (or roof) (in C); SC denotes the shading coefficient of the fenestration (or skylight); SF denotes the solar factor (in W/m^2); DT denotes the temperature difference between exterior and interior building environment; ΔT denotes the temperature difference between exterior and interior design conditions.

The PAL was first introduced by Japan which measures the total annual heating and cooling requirement in perimeter of the building for unit area [170,171]. The PAL is defined as follows

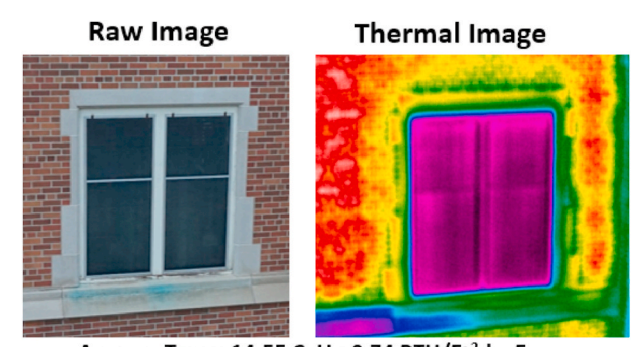


(b) Museum vs Twamley wall average wall U_c analysis

Fig. 9. U-value analysis of windows and walls (March 17th, 2020 morning).

 $PAL = (Annual thermal load of the inside perimeter zone (MJ/year)) / (Total floor area of the inside ambient space of each floor <math>(m^2)$)





Average Temp: 14.55 C, U_c: 0.74 BTU/Ft²-hr-F Single pane window

Fig. 10. Twamley window 1: Single pane (temperature/U-value) captured on October 9, 2019.

The *Envload* is a similar coefficient and used to estimate the cooling requirement for unit building area, and is defined as follows

$$ENVLOAD = a_0 + a_1 + \frac{\sum_{i=1}^{n} A_i \times K_i \times U_i \times IH_i}{A_{em}}$$
(36)

where a_0 and a_1 are the constants. A_i denotes the area of the i^{th} window (m^2) ; K denotes the modified factor for exterior shading devices; U_i denotes the heat transmittance of i^{th} window glass; IH is the annual solar radiation (kWh/m2); and Aen is the total area of the building envelope (m2). The OBEM is similar to ENVLOAD but applicable to office buildings as follows [165].

$$OBEM = -20370 + 2.010 \times G + 0.033 \times \left(\sum_{i}^{T_{i}} L_{i} \times DH\right) + 1.079 \times \left(\sum_{k}^{4} \sum_{i}^{T_{i}} Mk_{i} \times IH_{k}\right)$$

$$(37)$$

where G, L_i, T_i , and DH respectively denotes annual indoor heat gain, $W - h/m^2yr$, heat loss coefficient of building envelope in the i^{th} sector, W/m^2K , sectors number of the building envelope, and DH denotes annual degree-hours based on monthly average temperature (298 K), K - h/yr. Moreover, DH and IH_k are affected by the building orientation and location, where IH_k and MK_i denotes the isolation-hours $(W - h/m^2 - yr)$ and isolation gain coefficient on k^{th} orientation and i^{th} sector of the building.

The quantitative assessment of thermal performance depends on various factors including (i) layout or the structure of the building, (ii) type of material and its thermal properties, (iii) amount of water content or moisture present in the materials, (iv) age of the materials, and (v) alignment of different materials to form a complex structure of the building [34,108].

The IR measurements need to be taken in the absence of solar radiation or when it has the least effect such as during dawn or cloudy weather [84,172]. Ideally, the temperature difference is maintained as 10-15 K between internal and external environment [123]. This can be adjusted up to 7-16K [123] while maintaining accuracy. Table 8 shows the list of recommendations for thermal image capturing. The equations that estimate U-value consists of two components, (i) radiative and (ii)

convective components (see Eqs. (25), (27) and (43)). The radiative term is obtained using Stefan-Boltzmann equation. The convective term is different in various estimation techniques. In order to capture the convective component, the wind velocity is measured using an anemometer [125]. The convective component can also contain the length of the wall (see Eqs. (25), (27)). In Refs. [3,63,123,125,136], Hygrometers are used to measure the water vapour content in Ref. [139, 140].

The emissivity of the surface can be obtained from the data-sheet or using black tape [33,122,137]. Use of black tape requires additional efforts compared to using a data-sheet. In this method, the temperature of the material is measured adding a black tape and setting emissivity to 0.95. The emissivity that offers the same temperature of the surface after removing the black tape is the emissivity of the surface. The aluminum foil or mirrors are used to measure the reflected temperature [33, 121–123,137,139].

Assessment of the glazing system (or windows) is difficult compared to the other elements in a building. Glass is opaque in the long wave IR field and its thermal performance assessment using IR camera is difficult due to its high (almost 1.0) emissivity and can result in measurement errors [44,115,173,174].

Reflexive properties of the surrounding objects [175] and effect of air



Average Temp: 9.21 C, U-value: 0.18 BTU/Ft²-hr-F

Fig. 11. Museum window 1: Double pane (temperature/U-value) captured on October 8, 2019.

Double pane window

Table 13Twamley region-wise average temperature analysis.

	Left	Middle	Right	Avg
Upper	14.56	14.65	17.75	15.65
Middle	11.73	11.71	11.73	11.72
Bottom	14.29	14.27	15.23	14.60
Avg	13.53	13.54	14.90	-

 Table 14

 Museum region-wise average wall temperature analysis.

	Left	Middle	Right	Avg
Upper	9.02	8.96	8.72	8.9
Middle	8.38	8.59	11.75	9.57
Bottom	7.58	9.09	15.8	10.82
Avg	8.33	8.88	12.09	-

temperature [175] can also increase the measurement inaccuracies. In order to avoid these errors, the following corrective measures are proposed in Refs. [173–175]: (1) use of internal qualitative measurement (or indoor, controlled environment) instead of external qualitative measurement; (2) use of high emissivity materials like black tape and electric tape, as reference to estimate emissivity; and (3) maintaining a temperature difference of 15°C between the inside and outside walls [173–175]. These measurements are generally performed in the absence of solar radiation or when it has the least effect such as during dawn or cloudy weather [18,34,108,109,172,176]. Additional techniques were used to improve the measurement accuracy such as (1) sonic trials to estimate the overall wall density [84]; (2) ultrasonic devices to assess the structural defects [177,178]; (3) gravimetric tests to determine the water content present in the wall [101]; (4) chemical investigation to identify the chemical components present in the wall [61,179–181].

4. Data-driven three-layered framework

There are several methods for thermal assessment of buildings discussed in the literature. However, infrared thermal imagery seems to be promising due to its extensive features, high performance abilities, and relatively cheaper cost. Nevertheless, some intricacies exist in IRT imagery and requires a deeper understanding of different parameters that could influence the measurement results. IRT requires a knowledge of construction materials and thermodynamic properties of building

elements, various environmental parameters, and distance between camera and test specimen.

However, the thermal images must be pre-processed and automated before collecting any meaningful information. This includes removal of unwanted background objects and detection of the inspected specimen such as window, door, and wall, etc. However, limited contribution exists in the current literature in terms of automating the methods for background removal, object detection and U-value estimation. This lack of contribution motivates us to propose a fully automated method for U-value estimation of a building and its elements. Fig. 6 shows a data-driven approach for thermal performance assessment of building envelope.

The raw thermal imagery captured from various sources (e.g. aerial/ground measurement) are stored in a data repository (database layer). The images are fed into a pre-processing and automation layer, where a series of background elimination steps are undertaken, and the important features from the thermal images are extracted (refer Fig. 6); different elements of a building such as doors, roofs, facades, beams, and windows, are annotated and this dataset is used for training the machine learning models for object detection. Finally, the heat loss (U-value) of a building elements/envelope is quantified in the evaluation layer while considering the influential parameters (emissivity and reflected temperature).

4.1. Database layer

Thermal images of different buildings of University of North Dakota (UND) campus were collected to form a dataset of approximately 5000 thermal images (refer Table 9 and Fig. 5). These images were collected using a drone equipped with a Mirage 650 OGI sensor on different days. Initial datasets for machine learning and U-value estimation consisted of FLIR images but a gradual shift was made to using OGI images (primarily for U-value estimations) due to its higher precision and consistency in measurements. A HOBO sensor was used to collect the inside and outside building ambient air temperatures. Moreover, thermocouples were used to verify the surface temperatures obtained from thermal images. The environmental parameters (such as wind speed, air temperature) were obtained from Wunderground website [182]. The database layer also contains the building energy consumption data, which can be used further to validate the total heat-loss obtained using thermal images. Moreover, the database layer is responsible for housing all of the relevant data for training and testing our models. Further verification can be obtained using the Computer Aided Design (CAD) models. The database

Table 15Museum U-value estimation (evening) on October 8, 2019.

		Tempe	rature An	alysis		U-value Analysis					
		Surface temperature									
Building elements	# images	Max	Min	Avg	Thermocouple temperature	External Air temperature	$\overline{\mathbf{U}_1}$	\mathbf{U}_2	\mathbf{U}_3	\mathbf{U}_c	ASHRAE
Window 1	26	10.0	6.78	9.21	18 C	15 C	0.33	0.11	0.10	0.18	0.35
Window (all)	339	13.6	9.5	11.89			0.41	0.14	0.14	0.23	0.35
Wall 1	435	13.4	6.5	9.3			0.84	0.69	0.26	0.26	0.085
Roof	184	13.9	5.14	7.0			0	0	0	0	0.04

Table 16Twamley U-value estimation (morning), October 9, 2019.

		Tempera	ture Analy	sis			U-valu						
		Surface	Surface temperature										
Building elements	# images	Max	Min	Avg	Thermocouple temperature	Air temperature	U1	U2	U3	Uc	ASHRAE		
Window 1	26	17.84	13.49	14.55	7.9 C	6.3	0.77	0.74	0.71	0.74	0.95		
Windows (all)	1333	25.25	4.23	12.93			1.36	0.48	0.46	0.77	0.95		
Wall 1	1396	24.18	4.30	12.85			0.71	0.69	0.66	0.69	0.085		
Roof	174	2.64	0.26	1.3			0	0	0	0	0.04		

Table 17 Twamley U-value estimation (morning) on March 17, 2020.

		Tempera	ture Analys	is			U-value Analysis				
		Surface t	emperature	!							
Building Elements	# images	Max	Min	Avg	Thermocouple temperature	Air temperature	U1	U2	U3	Uc	ASHRAE
Window 1	5	-2.90	-5.89	-4.54	NA	−7.0 C	0.84	0.26	0.25	0.45	0.95
Windows in Face 1	334	-3.80	-5.53	-4.88			0.82	0.26	0.25	0.44	
Windows in Face 2	59	-3.87	-5.69	-5.12			0.80	0.25	0.24	0.43	
Windows in Face 3	87	-3.28	-5.73	-4.98			0.81	0.25	0.24	0.44	
Windows in Face 4	288	-5.54	-6.60	-6.14			0.69	0.21	0.21	0.37	
All Windows	779	-0.95	-6.99	-5.40			0.77	0.24	0.23	0.41	
Wall 1	114	-3.92	-5.58	-4.94	-2		0.68	0.22	0.21	0.37	0.085
Wall 2	38	-2.91	-5.79	-4.71			0.67	0.21	0.20	0.36	
Wall 3	51	-3.26	-5.65	-4.91			0.66	0.21	0.20	0.36	
Wall 4	52	-5.64	-6.60	-6.17			0.55	0.17	0.16	0.29	
Walls	262	-0.76	-7.07	-5.24			0.64	0.20	0.19	0.35	
Roof	62	15.12	-7.71	-4.87	NA		0.88	0.28	0.27	0.47	0.04

layer stores the raw and annotated datasets, models and their iterations, logs, and evaluation results. For redundancy purposes, copies of the models and dataset are stored on the High-performance Computing (HPC) clusters and Supervisely servers [183].

4.2. Pre-processing and automation layer

The pre-processing and automation layer is responsible for tasks such as background elimination, object detection, and instance classification that are required to extract meaningful insights from thermal imagery.

4.2.1. Background elimination

Presence of unwanted objects such as trees, grounds, sky etc. can interfere with the heat-loss estimation of the building. The authors of this paper have already carried out work on the background elimination of thermal images using Canny based Edge Detection (CED) and Dominant Color Isolation (DCI) [97]. The CED method uses first-order directional Gaussian derivatives to find edges by linking high-gradient pixels. This method extracts useful structural information from the grey scale images. This technique performs well when the objects are visually distinctive, such as the building wall and the sky (refer Fig. 8), but fails to perform when indistinct objects, like trees, windows, and doors, are present. Image 118 is an example when the edge detection method produces bad results. Dominant Color Masking (DCM) technique separates the image into DCMs and masks the remaining channels by binarizing the image. This technique computes the euclidean distance between colors in LAB Color space, where L is the lightness or approximate luminance, A is the first color parameter, green (negative) to magenta (positive) and B is the second color parameter, blue (negative)

to yellow (positive) forming the vector L,A,B, and A, B are in the range of \pm 1. DCM performs relatively better than CED when indistinct objects are present in the image.

The following metrics were used to evaluate the performance of these two approaches:

$$False \ positives = \frac{Pixels \ incorrectly \ removed}{Total \ number \ of \ pixels}$$
 (38)

$$False \ negatives = \frac{Pixels \ incorrectly \ remain}{Total \ number \ of \ pixels}$$
(39)

The accuracy of the CED and DCI methods in terms of these indices is compared in Table 10. CED produces much fewer False Positives (FP) as compared to the number of False Negatives (FN) for image 192. It also shows that DCI produces fewer FPs than FNs in all three cases. It can be observed that the total error rates using DCI on Image 192 was slightly lower than the edge detection method, and the number of false positives was lower using edge detection. Moreover, DCI has more FPs but fewer FNs. In summary, DCI performs better than canny edge detection (Table 10).

4.2.2. Instance segmentation

In order to accurately quantify the heat-loss, we need to detect different elements (such as doors, windows, walls etc.) of a building. In this work, we use machine learning based object detection techniques to accurately identify building elements. Moreover, after detecting the object it is necessary to identify the corresponding pixels in a thermal image. In order to achieve pixel-by-pixel classification, we needed a machine learning model that is capable of accomplishing instance

Table 18 Twamley U-value estimation (afternoon) on March 17, 2020.

		Tempera	ature Analys	is							
		Surface	temperature	:			U-valu				
Building Elements	# images	Max	Min	Avg	Thermocouple temperature	Air temperature	U1	U2	U3	Uc	ASHRAE
Window 1	11	54.32	12.50	25.09	NA	3.1 C	3.04	1.48	1.39	1.95	0.95
Windows in Face 1	295	60.18	12.11	28.35			3.51	1.75	1.55	2.28	
Windows in Face 2	79	52.18	1.28	18.23			2.09	1.01	0.92	1.34	
Windows in Face 3	84	54.01	-0.19	3.82			0.09	0.04	0.03	0.05	
Windows in Face 4	200	38.05	-0.57	9.58			1.09	0.5	0.46	0.68	
All Windows	723	60.18	-0.57	18.19			2.09	1.02	0.92	1.34	
Wall 1	43	60.18	9.01	33.83	−23.7 C		5.20	3.09	2.55	3.62	0.085
Wall 2	34	60.18	-7.26	17.69			3.06	1.67	1.44	2.06	
Wall 3	62	54.68	-0.19	4.35			0.80	0.36	0.34	0.50	
Wall 4	55	57.12	-1.11	10.13			2.03	1	0.91	1.33	
All Walls	270	60.18	-7.20	18.24			3.90	2.18	1.85	2.64	
Roof	62	60.04	-1.40	19.90	NA	NA	2.37	1.26	1.09	1.57	0.04

Table 19 Twamley U-value estimation (evening) on March 17, 2020.

		Temper	rature Analy	rsis							
		Surface temperature				_	U-valu				
Building Elements	# images	Max	Min	Avg	Thermocouple temperature	Air temperature	U1	U2	U3	Uc	ASHRAE
Window 1	11	2.38	-1.19	-0.67	NA	-4.4 C	0.71	0.15	0.15	0.33	0.95
Windows in Face 1	279	3.16	-1.26	-0.29			0.78	0.16	0.16	0.37	
Windows in Face 2	33	7.29	-0.81	1.02			1.03	0.22	0.22	0.49	
Windows in Face 3	23	4.35	-0.98	0.14			0.86	0.18	0.18	0.41	
Windows in Face 4	167	2.72	-1.31	-0.61			0.72	0.15	0.15	0.34	
Windows in Face 5	132	3.51	-1.89	-1.09			0.63	0.13	0.13	0.30	
All Windows	645	4.21	-1.25	-0.16			0.80	0.17	0.17	0.38	
Wall 1	106	2.87	-1.24	-0.20	−7.5 C		1.42	0.32	0.30	0.68	0.085
Wall 2	35	6.60	-0.76	2.03			1.74	0.40	0.38	0.84	
Wall 3	13	4.77	-0.98	0.48			1.74	0.40	0.38	0.84	
Wall 4	68	3.95	-1.39	0.04			1.40	0.31	0.30	0.67	
Wall 5	70	3.22	-1.92	-1.06			1.43	0.32	0.31	0.69	
All Walls	292	4.28	-1.26	0.26			1.55	0.35	0.34	0.74	
Roof	82	2.48	-3.80	-2.11	NA	NA	0.43	0.09	0.09	0.20	0.04

segmentation. Instance segmentation is the combination of object detection, classifying objects and localizing with bounding boxes, and semantic segmentation. The semantic segmentation classifies objects with a pixel level association. Convolution Neural Network (CNN) is a type of Neural Network that performs extremely well for segmentation [184].

Mask R–CNN [185] is a supervised learning model, where the neural network learns from manually (human) annotated objects with the desired classes and tags. In order to organize the tremendous amount of data generated during annotations, training, and testing phases, we used a web-based platform called Supervisely [183]. The Supervisely web-portal offers the ability for training (e.g. by providing the model name, labeled dataset, and hyper-parameters) and testing several models with very few interactions. Supervisely provides a convenient Data Transformation Language (DTL) to easily manipulate datasets. We used the DTL feature to augment and split the data set into training and validation sets.

Fig. 7 demonstrates an end-to-end pipeline starting from user requests to U-value evaluation. First, the user requests a task to be performed on a dataset which gets sent to the database layer. This layer keeps a running track of all tasks requested. If the user requests a model to be trained, the task gets relayed to the Supervisely platform. This platform keeps track of all the model weights and logs. If the requested task is a 'testing', the automation layer gets triggered, then the model metrics such as mean Average Precision (mAP) and mean Intersection over Union (mIoU) are computed. These results are then uploaded to the supervisely platform. Wall temperature is collected from the CSV's, the building dimensions from architectural blueprints, weather data from wunderground [182] database, and object coordinates from the JSON file. These external parameters are brought in for the U-value assessment

in the evaluation layer.

4.3. Evaluation layer

The evaluation layer consists of testing the Mask R–CNN model on a particular dataset, and extracting the ROI's to compute the relevant heat-loss or U-values with respect to the object identified by the model.

$$Precision = \frac{TP}{(TP + FP)} \tag{40}$$

$$Recall = \frac{TP}{(TP + FN)} \tag{41}$$

The *Precision* denotes the accuracy of the predictions and expressed as a percentage of True Positives (TP) and Total Positives which is the summation of TP and False Positives (FP) [189]. Whereas, *Recall* is estimated as the ratio of TP and, FP and False Negatives (FN).

$$IoU = \frac{Area \quad of \quad overlap}{Area \quad of \quad union} \tag{42}$$

IoU is a widely used metric to evaluate semantic segmentation, and image segmentation, applications [186]. The IoU denotes a percentage of pixels that overlap over between the model's annotation and ground truth over all of the pixels occupied by both of the annotations.

5. Results and discussion

5.1. Instance segmentation

In order to train the thermal images, a polygon tool (provided by Supervisely [183]) was used for annotation to mark the silhouette of the

Table 20 Museum U-value estimation (morning) on March 17, 2020.

		Temper	ature Anal	ysis			U-valu				
	# images	Surface	temperatu	re		_					
Building Elements		Max	Min	Avg	Thermocouple temperature	Air temperature	U1	U2	U3	Uc	ASHRAE
Window 1	28	-1.6	-5.9	-4	NA	−11 C	0.5	0.196	0.19	0.29	0.35
Windows in Face 1	166	0.36	-6.4	-5.1		−11 C	0.42	0.16	0.15	0.24	
Windows in Face 2	155	3	-7	-4.1		-11 C	0.49	0.19	0.18	0.29	
All Windows	321	3	-7	-4.6		-11 C	0.46	0.177	0.172	0.27	
Wall 1	107	6.1	-6.8	-5.4	−4.7 C	-11 C	0.33	0.130	0.126	0.1	0.085
Wall 2	126	3	-7	-4.3		-11 C	0.34	0.133	0.13	0.2	
All Walls	233	6.1	-7	-4.7		−11 C	0.34	0.133	0.130	0.20	
Roof	121	5.5	-7.9	-6.3	NA	NA	0.33	0.41	0.12	0.12	0.04

Table 21
Museum U-value estimation (afternoon) on March 17, 2020.

		Tempera	ture Analys	sis			U-value Analysis					
		Surface temperature										
Building Elements	# images	Max	Min	Avg	Thermocouple temperature	Air temperature	U1	U2	U3	Uc	ASHRAE	
Window 1	18	14.51	2.89	7.02	NA	3.1 C	0.5	0.196	0.19	0.29	0.35	
Windows in Face 1	217	23.49	2.32	7.03		3.1 C	0.62	0.25	0.24	0.37		
Windows in Face 2	184	30.6	0.3	7.09		3.1 C	0.63	0.28	0.26	0.39		
All Windows	402	60.18	0.3	7.06		3.1 C	0.62	0.26	0.25	0.38		
Wall 1	114	19.41	2.32	7.54	20.0 C	3.1 C	0.96	0.39	0.38	0.58	0.085	
Wall 2	98	60.18	-1.7	8.46		3.1 C	1.57	0.72	0.68	1		
All Walls	213	60.18	-1.7	7.97		3.1 C	1.25	0.54	0.52	0.77		
Roof	38	60.18	-2.24	12.47	NA	3.1 C	1.52	0.73	0.67	0.97	0.04	

object of interest (facades, windows, and roofs), and then subsequently tagged by its name. These annotations are converted into a JSON (JavaScript Object Notation) format that is readable by the Mask R-CNN model. The overall structure of JSON file consists of each identified object, classTitles, followed by the co-ordinates populated by each of these objects. The Mask R-CNN model was trained on the Microsoft COCO dataset. This dataset consists of 1.5 million object instances with 80 object categories. Due to initial smaller size of our dataset, we chose to employ transfer-learning rather than training our model on our own custom dataset. In transfer learning, the pre-trained weights of the COCO dataset could be used as initialization weights and the model is retrained and re-purposed. One problem of small datasets is over-fitting, and to overcome this issue, data augmentation was applied. Using the DTL API, three different types of transformations were applied: a vertical flip transformation is applied first, followed by a multiply transformation that makes an exact copy of the image, and a crop filter that was added with a minimum crop width and height of 70% with a maximum crop of 90%. The three augmentations multiplied the dataset, on average, by a factor of 22 (over 100,000 images in the augmented

The training of the Mask R–CNN model was accomplished on a High Performance Computer (HPC) with NVidia RTX 2080Ti graphics card. Supervisely provides a Docker image that links the HPC cluster to the Web API. We are able to run the specified model and dataset on the HPC while uploading results to Supervisely as specified by the configuration file. Within this configuration file, the hyper-parameters— such as learning rate, input resolution, number of GPU's, and epochs— are specified. These hyper-parameters were held constant throughout each training session, except for learning rate, as illustrated in Table 11. However, the optimal number of epochs to train the models is challenging to determine. One way to determine the number of epochs required is to observe the loss function which will eventually start to converge on a value. The input dimensions for the model were set to 256x256 and the batch size was set to train on one image and validate on one image.

In order to evaluate the Mask R–CNN model, we built our test dataset which consists of 54 FLIR images and 102 OGI images. At the end of each training session the best performing model's (lowest loss) weights are saved in a.h5 file and used for inferencing. The coordinates calculated by the mask are then saved within a JSON file.

The Mask R–CNN model was evaluated on its accuracy of object detection and mask (refer Table 12). The model was trained on FLIR images and tested on a dataset containing both 54 FLIR and 102 OGI images. Overall the average precision, at confidence level of 0.50, for windows is 0.67 and facade is 0.46 with a mean average precision of 0.56. The detection of windows out performs the detection of facades, but the accuracy of the mask for windows is low. When evaluating the mask accuracy of facades we are able to achieve 0.50.

5.2. Heat loss estimation via surface temperature analysis

The raw thermal images were analyzed using IR Flash Pro software to extract the temperature data. For an accurate U-value estimation, we used the manual annotated images instead of the direct software annotation from the Mask R-CNN model. This is due to the fact that there is still not a 100% detection accuracy on the masks or instances. The preliminary results analyzed buildings from direct annotated U values from Mask R-CNN are yet closer to manually done annotated images. For reliability and completeness of the estimation of surface temperature estimation, we used actual surface temperature for the entire objects such as windows, facades, walls and roofs. The U-value trend for the single-pane and double-pane windows are shown in Fig. 9. Twamley Hall's windows at the UND campus are single-pane windows whereas the windows at the Musuem are of double-pane. The double pane windows are more efficient than single pane windows in insulating the heat-flow. The results correlates with this assessment as U-values correspond to single pane are higher than double pane windows (refer Fig. 9). The average temperature for single-pane and double-pane windows are 12.85 and 9.21 °C, respectively (refer Fig. 10 and Fig. 11).

In order to capture the temperature profile of different sections of the

Table 22 Museum U-value estimation (evening) on March 17, 2020.

		Temper	ature Anal	ysis			U-value Analysis				
		Surface temperature									
Building Elements	# images	Max	Min	Avg	Thermocouple temperature	Air temperature	U1	U2	U3	Uc	ASHRAE
Window 1	29	-2.7	-2.2	0.5	NA	-4 C	0.41	0.162	0.158	0.24	0.35
Windows in Face 1	128	8.6	-3	0.1		−4 C	0.38	0.14	0.14	0.22	
Windows in Face 2	136	11.5	-0.5	3.8		−4 C	0.62	0.249	0.241	0.37	
All Windows	264	11.5	-0.5	2.03		−4 C	0.56	0.22	0.21	0.33	
Wall 1	115	5.1	-2.6	0.05	1.2 C	−4 C	0.4	0.158	0.155	0.24	0.085
Wall 2	110	11.5	-2.8	3.9		-4 C	0.59	0.24	0.23	0.35	
All Walls	225	11.5	-2.8	1.9		−4 C	0.44	0.180	0.175	0.26	
Roof	65	4.2	-3.3	-0.9	NA	−4 C	0.28	0.107	0.105	0.16	0.04

wall, we show the average temperature of corresponding sections in Table 13 and Table 14. Table 13 shows that the upper-right section of Twamley encounters maximum heat loss, whereas Table 14 shows the bottom-right section of the Museum building encounters maximum heat loss. The emissivity, outside and inside air temperature, and wind velocities were captured to accurately estimate the U-values. The outdoor temperature was obtained from the HOBO sensor embedded in the drone. A weather data site called Wunderground was used [182] to gather wind velocity. Following equations are used to quantify the heat loss transmittance coefficient.

$$U_{1} = \frac{\varepsilon\sigma(T_{se}^{4} - T_{ae}^{4}) + 3.805v(T_{se} - T_{ae})}{T_{ai} - T_{ae}}$$
(43)

$$U_2 = \frac{4\varepsilon\sigma T_s^3 \left(T_{si} - T_{refl}\right) + \alpha_c \left(T_{si} - T_{ai}\right)}{T_{ai} - T_{ae}} \tag{44}$$

$$U_{3} = \frac{4\varepsilon\sigma T_{m}^{3} \left(T_{si} - T_{refl}\right) + \alpha_{c} \left(T_{si} - T_{ai}\right)}{T_{ai} - T_{ae}}$$

$$\tag{45}$$

$$U_c = \frac{U_1 + U_2 + U_3}{3} \tag{46}$$

where ν is the velocity of external wind, T_s is the surface temperature, $T_m = \frac{T_s + T_{refl}}{2}$ denotes the mean temperature, $\alpha_c = c_1 \frac{(T_{sl} - T_{al})^{\frac{1}{4}}}{L}$ denotes the convective heat transmittance coefficient, and U_c denotes the cumulative U-value. We set the Stefan-Boltzmann constant $\sigma = 5.67 \times 10^{-8} \ Wm^{-2}K^{-1}$ and emissivity $\varepsilon = 0.75$ for walls and 1.0 for windows. The surface temperatures $(T_{si}$ and $T_{se})$ were obtained using the thermal images. The building height information is noted from the architectural diagram.

Tables 15 and 20–22 show the U-values (U_1 , U_2 , U_3 , U_c) and compared with the ASHRAE standard data (in BTU/hr °F ft^2) for the Museum building in UND campus. These tables also contain the building element type, the total number of images analyzed, the minimum, maximum, and average surface temperatures, thermocouple temperature obtained from the building surface, and the air temperature from weather data. Similarly, Tables 16–19 show the U-values and related parameters for UND's Twamley building. The U-value results indicate that single-pane windows (i.e. Twamley building) are less efficient than the double-pane windows (i.e. Museum building). Moreover, the afternoon U-values are higher than the morning and evening U-values due to the effect of sunlight. We also noticed that the window U_1 values are more consistent with the ASHRAE standard, whereas the wall U_3 values are more consistent with the ASHRAE standard.

6. Conclusion

A detailed evaluation of heat loss measurement types, processes, and methods (e.g., both qualitative and quantitative) of IRT/non-IRT approaches are discussed. Specifically, a novel three-layered framework with an application of an instance segmentation method (i.e., Mask R-CNN) was investigated. Estimations of U-value for multiple objects of buildings (e.g., facades, walls, windows, and roofs) are calculated. The U-value results show that the UAV-assisted thermal imagery-based heatloss estimation can effectively distinguish between single and double pane windows and also consistent with the ASHRAE standards. The Twamley windows are single pane (Avg U-value: approx. 0.9) whereas the Museum windows are double pane (avg U-value: approx. 0.3). Heat loss estimation for the walls is not consistent with the ASHRAE standard. However, the thermal imagery-based techniques are efficient to identify the old and new building walls. The U-values for the Twamley walls (old) are consistently higher than Museum walls (relatively new). Moreover, the afternoon U-values are unacceptable due to the solar irradiance effects which confirms that surface free from any incident solar radiation is the most suitable for thermal imagery data.

7. Future work

The future work includes (1) improving the automation of instance segmentation models and estimating surface temperatures seamlessly in real-time; (2) correlating thermal assessment of multiple UAS imagery of same building over different seasons and with energy consumption and material data of buildings and (3) hotspot detection via pixel-by-pixel analysis; (4) full automation of the data capturing process wherein building inspections can be carried out remotely with little to no human intervention by setting pre-determined flight paths [187] (5) real-time 3D modeling (e.g., using point clouds); of the inspected building(s) through the combined use of the captured 2D thermal and color images through monocular thermography to offload post-processing computational loads; and (6) the recruitment of a ground-based vehicle to be used in tandem with a UAV that acts as a charging station for the UAV to make large-scale inspections more feasible on a single run [188].

CRediT author statement

Debanjan Sadhukhan: Writing - original draft, Methodology, Software, Data curation, Visualization, Validation, Writing - review & editing. Sai Peri: Software, Writing, Data curation, Visualization, Investigation. Niroop Sugunaraj: Software, Data curation, Visualization, Investigation, Writing - review & editing. Avhishek Biswas: Software, Data curation, Visualization. Daisy Flora Selvaraj: Writing - review & editing, Methodology. Katelyn Koiner: Software, Methodology, Writing - review & editing, Writing - original draft. Andrew Rosener: Software, Methodology, Writing - review & editing, Writing - review & editing. David Flynn: Conceptualization, Writing - review & editing. Prakash Ranganathan: Conceptualization, Methodology, Supervision, Project administration, Funding acquisition, Writing - review & editing, Resources, Formal analysis.

Declaration of competing interest

The authors declare that they have no known competing interests or personal relationships that could have appeared to influence the work reported in this paper.

Acknowledgement

The authors acknowledge the support from our collaborators such as North Dakota Department of Commerce (Award # UND0022166), SkySkopes, Inc, VPR office at the UND, university system office for enabling acquisition of thermal images in the 11 campuses at NDUS, Michael Nord, Building Faciliies Manager, and Dr. Gautham Krishnamoorthy, Professor of Chemical Engineering at the UND campus.

Appendix A. Supplementary data

Supplementary data to this article can be found online at https://doi.org/10.1016/j.jobe.2020.101637.

References

- O. Kaynakli, A review of the economical and optimum thermal insulation thickness for building applications, Renew. Sustain. Energy Rev. 16 (1) (2012) 415–425
- [2] J. Lee, J. Kim, D. Song, J. Kim, C. Jang, Impact of external insulation and internal thermal density upon energy consumption of buildings in a temperate climate with four distinct seasons, Renew. Sustain. Energy Rev. 75 (2017) 1081–1088.
- [3] L. Aditya, T. Mahlia, B. Rismanchi, H. Ng, M. Hasan, H. Metselaar, O. Muraza, H. Aditiya, A review on insulation materials for energy conservation in buildings, Renew. Sustain. Energy Rev. 73 (2017) 1352–1365.
- [4] S. Grammatikos, E. Kordatos, T. Matikas, C. David, A. Paipetis, Current injection phase thermography for low-velocity impact damage identification in composite laminates, Mater. Des. 55 (2014) 429–441.

- [5] C. Ibarra Castanedo, J.M. Piau, S. Guilbert, N.P. Avdelidis, M. Genest, A. Bendada, X.P. Maldague, Comparative study of active thermography techniques for the nondestructive evaluation of honeycomb structures, Res. Nondestr. Eval. 20 (1) (2009) 1–31.
- [6] N. Nazaryan, C. Campana, S. Moslehpour, D. Shetty, Application of a he3ne infrared laser source for detection of geometrical dimensions of cracks and scratches on finished surfaces of metals, Optic Laser. Eng. 51 (12) (2013) 1360–1367.
- [7] Y.K. An, J. Yang, S. Hwang, H. Sohn, Line laser lock in thermography for instantaneous imaging of cracks in semiconductor chips, Optic Laser. Eng. 73 (2015) 128–136.
- [8] Residential energy services network (resnet), Interim Guidelines for Thermographic Inspections of Buildings. Resnet, 2012.
- [9] American society for testing and materials (astm), Standard Practice for Thermographic Inspection of Insulation Installations in Envelope Cavities of Frame Buildings. West Conshohocken: Astm, 1997.
- [10] European committee for standardization (cen), thermal performance of buildings, qualitative detection of thermal irregularities in building envelopes, infrared method, standard en 13187, cen, brussels, 1998.
- [11] International organization for standardization (iso), Condition Monitoring and Diagnostics of Machines. Thermography, Standard 18434, Iso, Geneve, 2008.
- [12] American society for testing and materials (astm), standard test method for minimum resolvable temperature difference for thermal imaging systems, e 1213, astm, west conshohocken, 2009.
- [13] American society for testing and materials (astm), standard test methods for measuring and compensating for emissivity using infrared imaging radiometers, e 1933, astm, west conshohocken, 2005.
- [14] American society for testing and materials (astm), Standard Test Method for Minimum Detectable Temperature Difference for Thermal Imaging Systems, 1311, Astm, West Conshohocken, 2004.
- [15] American society for testing and materials (astm), standard test method for measuring and compensating for reflected temperature using infrared imaging radiometers, e 1862, astm, west conshohocken, 1997.
- [16] American society for testing and materials (astm), standard guide for examining electrical and mechanical equipment with infrared thermography, e 1934, astm, west conshohocken, 2005.
- [17] American society for testing and materials (astm), Standard Practice for Thermographic Inspection of Insulation Installations in Envelope Cavitiesof Frame Buildings, C 1060 11, Astm, West Conshohocken, 1997.
- [18] C. Pearson, Thermal Imaging of Building Fabric, Bisra Guide Bg39, 2011.
- [19] E. Lucchi, Applications of the infrared thermography in the energy audit of buildings: a review. Renew. Sustain. Energy Rev. 82 (2018) 3077–3090.
- [20] H. Kayan, R. Eslampanah, F. Yeganli, M. Askar, Heat leakage detection and surveiallance using aerial thermography drone, in: 2018 26th Signal Processing and Communications Applications Conference (SIU), 2018, pp. 1–4.
- [21] A.A. Muresan, S. Attia, Energy efficiency in the Romanian residential building stock: a literature review, Renew. Sustain. Energy Rev. 74 (2017) 349–363.
- [22] B. P. I. E. (BPIE), Europeé Buildings under the Microscope, a Country-By-Country Review of the Energy Performance of Buildings, 2011.
- [23] F. Ascione, N. Bianco, R.F. De Masi, G.M. Mauro, M. Musto, G.P. Vanoli, Experimental validation of a numerical code by thin film heat flux sensors for the resolution of thermal bridges in dynamic conditions, Appl. Energy 124 (2014) 213–222
- [24] F. Ascione, F. Ceroni, R.F. De Masi, F. de Rossi, M.R. Pecce, Historical buildings: multidisciplinary approach to structural/energy diagnosis and performance assessment, Appl. Energy 185 (2017) 1517–1528.
- [25] P.G. Cesaratto, M. De Carli, A measuring campaign of thermal conductance in situ and possible impacts on net energy demand in buildings, Energy Build. 59 (2013) 29–36.
- [26] J. Siviour, Experimental u-values of some house walls, Build. Serv. Eng. Technol. 15 (1) (1994) 35–36.
- [27] E. Lucchi, Diagnosi Energetica Strumentale Degli Edifici, Dario Flaccovio Editore, Palermo, 2012.
- [28] S. Doran, E. Kilbride, Safety and Health Business Plan, Field Investigations of the Thermal Performance of Construction Elements as Built, 2000.
 [29] S. Rhee-Duverne, P. Baker, Research into the Thermal Performance of Traditional
- [29] S. Rhee-Duverne, P. Baker, Research into the Thermal Performance of Traditional Brick Walls, English Heritage, London, 2013.
- [30] E. Lucchi, Thermal transmittance of historical stone masonries: a comparison among standard, calculated and measured data, Energy Build. 151 (2017) 393-405
- [31] B. Abad, D.A. Borca Tasciuc, M. Martin Gonzalez, Non contact methods for thermal properties measurement, Renew. Sustain. Energy Rev. 76 (2017) 1348–1370.
- [32] B. ISO, et al., Building Materials and Products Hygrothermal Properties Tabulated Design Values and Procedures for Determining Declared and Design Thermal Values, 2007.
- [33] P.A. Fokaides, S.A. Kalogirou, Application of infrared thermography for the determination of the overall heat transfer coefficient (u value) in building envelopes, Appl. Energy 88 (12) (2011) 4358–4365.
- [34] Residential Energy Services Network (RESNET), Interim Guidelines for Thermographic Inspections of buildings., RESNET, 2012.
- [35] C. Koo, S. Park, T. Hong, H.S. Park, An estimation model for the heating and cooling demand of a residential building with a different envelope design using the finite element method, Appl. Energy 115 (2014) 205–215.
- [36] V. Neela, A. De, Three-dimensional heat transfer analysis of lens tm process using finite element method, Int. J. Adv. Manuf. Technol. 45 (9–10) (2009) 935.

- [37] E. Grinzato, P. Bison, S. Marinetti, Monitoring of ancient buildings by the thermal method, J. Cult. Herit. 3 (1) (2002) 21–29.
- [38] N. Avdelidis, A. Moropoulou, Applications of infrared thermography for the investigation of historic structures, J. Cult. Herit. 5 (1) (2004) 119–127.
- [39] E. Barreira, R.M. Almeida, J. Delgado, Infrared thermography for assessing moisture related phenomena in building components, Construct. Build. Mater. 110 (2016) 251–269.
- [40] G.R. Stockton, Methodologies of Finding, Analyzing and Prioritizing Moisture Problems in Roofing Materials Using Infrared Thermal Imaging, IR/INFO 2013, 2013.
- [41] S.M. Ocaña, I.C. Guerrero, I.G. Requena, Thermographic survey of two rural buildings in Spain, Energy Build. 36 (6) (2004) 515–523.
- [42] M. Fox, S. Goodhew, P. De Wilde, Building defect detection: external versus internal thermography, Build. Environ. 105 (2016) 317–331.
- [43] E. Barreira, R.M. Almeida, M. Moreira, An infrared thermography passive approach to assess the effect of leakage points in buildings, Energy Build. 140 (2017) 224–235.
- [44] T. Taylor, J. Counsell, S. Gill, Energy efficiency is more than skin deep: improving construction quality control in new build housing using thermography, Energy Build. 66 (2013) 222–231.
- [45] H. Glavaš, L. Józsa, T. Barić, Infrared thermography in energy audit of electrical installations, Teh. Vjesn. 23 (5) (2016) 1533–1539.
- [46] C. Xu, N. Zhou, J. Xie, X. Gong, G. Chen, G. Song, Investigation on eddy current pulsed thermography to detect hidden cracks on corroded metal surface, NDT E Int. 84 (2016) 27–35.
- [47] FLIR Camera Mounted, https://www.thinkdefence.co.uk/2014/02/future maritime patrol part 4 cheaper options/flir sensor lg/, [Online].
- [48] Controp, https://www.laserfocusworld.com/articles/2016/07/controp releases lightweight high definition eo ir camera payload for helicopters.html, [Online].
- [49] Yuneec Typhoon, https://us.yuneec.com/typhoon h overview, [Online].
- [50] FLIR Vehicle Lightweight Camera [Online], https://www.flir.eu/newscenter/military/flir lightweight vehicle surveillance system lvss/.
- [51] HT Portable Camera, , [Online].
- [52] R. Adhikari, E. Lucchi, V. Pracchi, Experimental measurements on thermal transmittance of the opaque vertical walls in the historical buildings proceedings of PLEA2012, in: 28th Conference, Opportunities, Limits & Needs towards an Environmentally Responsible Architecture, 2012, pp. 1248–1256.
- [53] P. Baker, U values and traditional buildings: in situ measurements and their comparisons to calculated values, Hist.Scotl.Tech. Pap. 10 (2011).
- [54] J. Bros Williamson, J. Stinson, C. Garnier, J. Currie, In situ monitoring of thermal refurbishment on pre 1919 properties in scotland, Int J Sustain Constr 2 (2014) 26–33.
- [55] C. rye, Spab Research Report n.1: U Value Report, Spab, London, 2011.
- [56] I. Nardi, T. de Rubeis, M. Taddei, D. Ambrosini, S. Sfarra, The energy efficiency challenge for a historical building undergone to seismic and energy refurbishment, Energy Procedia 133 (2017) 231–242.
- [57] M. Jiménez, B. Porcar, M. Heras, Application of different dynamic analysis approaches to the estimation of the building component u value, Build. Environ. 44 (2) (2009) 361–367.
- [58] A.H. Deconinck, S. Roels, Comparison of characterisation methods determining the thermal resistance of building components from onsite measurements, Energy Build. 130 (2016) 309–320.
- [59] E. Sassine, A practical method for in situ thermal characterization of walls, Case Stud.Therm. Eng. 8 (2016) 84–93.
- [60] K. Gaspar, M. Casals, M. Gangolells, In situ measurement of façades with a low u-value: avoiding deviations, Energy Build. 170 (2018) 61–73.
- [61] F. Asdrubali, G. Baldinelli, F. Bianchi, A quantitative methodology to evaluate thermal bridges in buildings, Appl. Energy 97 (2012) 365–373.
- [62] I.A. Atsonios, I.D. Mandilaras, D.A. Kontogeorgos, M.A. Founti, Two new methods for the in situ measurement of the overall thermal transmittance of cold frame lightweight steel framed walls, Energy Build. 170 (2018) 183–194.
- [63] R. Albatici, A. Tonelli, Verifica sperimentale in situ, con analisi termografiche e algoritmi di calcolo, della trasmittanza termica di un elemento costruttivo, Museo Civico di Rovereto: Rovereto, Italy (2008) 103–125.
- [64] P.G. Cesaratto, M. De Carli, S. Marinetti, Effect of different parameters on the in situ thermal conductance evaluation, Energy and buildings 43 (7) (2011) 1792–1801.
- [65] G. Ficco, F. Iannetta, E. Ianniello, F.R.d.A. Alfano, M. Dell Isola, U value in situ measurement for energy diagnosis of existing buildings, Energy Build. 104 (2015) 108–121.
- [66] M. Scarpa, P. Ruggeri, F. Peron, M. Celebrin, M. De Bei, New measurement procedure for u value assessment via heat flow meter, Energy Procedia 113 (2017) 174–181.
- [67] Astm international (american society for testing and materials), Standard Test Method for Steady State Heat Flux Measurements and Thermal Transmission Properties by Means of the Guarded Hot Plate Apparatus, Designation C177, Astm, West Conshohocken, 2013.
- [68] Iso (international organization for standardization), Thermal Insulation. Determination of Steady State Thermal Resistance and Related Properties. Heat Flow Meter Apparatus, Standard Iso 8301, Iso, Geneva, 2014.
- [69] sm Ocana, ic guerrero, ig requena, Thermographic survey of two rural buildings in Spain, Energy Build. 36 (6) (2004 Jun 1) 515–523.
- [70] T. Kobari, J. Okajima, A. Komiya, S. Maruyama, Development of guarded hot plate apparatus utilizing peltier module for precise thermal conductivity measurement of insulation materials, Int. J. Heat Mass Tran. 91 (2015) 1157–1166.

- [71] R. Ricciu, L.A. Besalduch, A. Galatioto, G. Ciulla, Thermal characterization of insulating materials, Renew. Sustain. Energy Rev. 82 (2018) 1765–1773.
- [72] C.S. Sanjaya, T.H. Wee, T. Tamilselvan, Regression analysis estimation of thermal conductivity using guarded hot plate apparatus, Appl. Therm. Eng. 31 (10) (2011) 1566–1575.
- [73] J. Wang, C. Demartino, Y. Xiao, Y. Li, Thermal insulation performance of bamboo and wood based shear walls in light frame buildings, Energy Build. 168 (2018) 167–179.
- [74] J. Sala, A. Urresti, K. Martín, I. Flores, A. Apaolaza, Static and dynamic thermal characterisation of a hollow brick wall: tests and numerical analysis, Energy Build. 40 (8) (2008) 1513–1520.
- [75] K.G. Wakili, C. Tanner, U-value of a dried wall made of perforated porous clay bricks: hot box measurement versus numerical analysis, Energy Build. 35 (7) (2003) 675–680.
- [76] D. Aviram, A. Fried, J. Roberts, Thermal properties of a variable cavity wall, Build. Environ. 36 (9) (2001) 1057–1072.
- [77] H. Kus, E. Özkan, Ö. Göcer, E. Edis, Hot box measurements of pumice aggregate concrete hollow block walls, Construct. Build. Mater. 38 (2013) 837–845.
- [78] E.H. Ridouane, M. Bianchi, Three dimensional numerical evaluation of thermal performance of uninsulated wall assemblies, Tech. rep., National Renewable Energy Lab. (NREL), Golden, CO (United States) NREL/CP-5500-52389 (2011) 1–10.
- [79] S. Ferrari, V. Zanotto, The thermal performance of walls under actual service conditions: evaluating the results of climatic chamber tests, Construct. Build. Mater. 43 (2013) 309–316.
- [80] Y. Gao, J. Roux, C. Teodosiu, L. Zhao, Reduced linear state model of hollow blocks walls, validation using hot box measurements, Energy Build. 36 (11) (2004) 1107–1115.
- [81] C. Ibarra Castanedo, J.R. Tarpani, X.P. Maldague, Nondestructive testing with thermography, Eur. J. Phys. 34 (6) (2013) S91.
- [82] C. pearson, Thermal Imaging of Building Fabric, Bisra Guide Bg39, Bisra, Bracknell, 2011.
- [83] I. Danielski, M. Froling, Diagnosis of buildings thermal performance a quantitative method using thermography under non steady state heat flow, Energy Procedia 83 (2015) 320–329.
- [84] E. Lucchi, Non invasive method for investigating energy and environmental performances in existing buildings, in: PLEA Conference on Passive and Low Energy Architecture. 2011.
- [85] G. Dall, E. Lucchi, G. Poliseno, Infrared scanning on buildings as a tool for evaluating pathologies and suggesting energy retrofit actions, in: 47th AiCARR International Conference on Systems, Energy and Built Environment toward a Sustainable Comfort, vol. 89, Tivoli, Roma, Italy, 2009.
- [86] A. Thumann, W.J. Younger, Handbook of energy audits, The Fairmont Press, Inc (2008).
- [87] B.M. Marino, N. Muñoz, L.P. Thomas, Estimation of the surface thermal resistances and heat loss by conduction using thermography, Appl. Therm. Eng. 114 (2017) 1213–1221.
- [88] A. Rogalski, Infrared detectors: status and trends, Prog. Quant. Electron. 27 (2–3) (2003) 59–210.
- [89] J.P. Miller, N. Singh, Kinetic super resolution long wave infrared (ksr lwir) thermography diagnostic for building envelopes: scott afb, il, Tech. rep.,Eng.Res. Dev.Cent.Champaign. IL .Construct. (2015) 1–53. EW-201241.
- [90] Essess Thermal Technology, 2017.
- [91] J. Armstrong, K. Butcher, J. Rowe, CIBSE Concise Handbook, Chartered Institution of Building Services Engineers, 2003.
- [92] A. Tibbs, Using Infrared Thermography to Assess Building Problems, Closer Look Inspections, Cleveland, OH, 2004.
- [93] J. Snell, M. Schwoegler, The use of infrared thermal imaging for home weatherization, The Snell Group (2012) 6.
- [94] Sagewell Inc, Cambridge [Online], https://www.sagewell.com/.
- [95] Projected2perform [Online], https://www.projected2perform.com/residential th ermal-imaging/.
- [96] SafetyHawaii [Online], http://www.safetywisehawaii.com/.
- [97] K. Koiner, A. Rosener, D. Sadhukhan, D.F. Selvaraj, Z.E. Mrabet, M. Dunlevy, P. Ranganathan, Heat loss estimation using uas thermal imagery, in: IEEE EIT 2019. IEEE, 2019.
- [98] A. Donatelli, P. Aversa, V.A.M. Luprano, Set up of an experimental procedure for the measurement of thermal transmittances via infrared thermography on lab made prototype walls, Infrared Phys. Technol. 79 (2016) 135–143.
- [99] J. Sun, Analysis of pulsed thermography methods for defect depth prediction, J. Heat Tran. 128 (4) (2006) 329–338.
- [100] A. Moropoulou, T. Tsiourva, K. Bisbikou, V. Tsantila, G. Biscontin, G. Longega, M. Groggia, E. Dalaklis, A. Petritaki, Evaluation of cleaning procedures on the facades of the bank of Greece historical building in the center of athens, Build. Environ. 37 (7) (2002) 753–760.
- [101] F. Luzi, M. Mitchell, C. Nanni, V. Redaelli, et al., Thermography: current status and advances in livestock animals and in veterinary medicine, Thermography: Curr.Status.Adv.Livest.Anim.Vet. Med. (2013) 1–236.
- [102] R.S. Adhikari, E. Lucchi, V. Pracchi, Experimental measurements on thermal transmittance of the opaque vertical walls in the historical buildings, in: Proceedings of PLEA2012. 28th Conference, Opportunities, Limits & Needs towards an Environmentally Responsible Architecture. Lima, 2012, pp. 1248–1256.
- [103] A. Muscio, P.G. Bison, S. Marinetti, E. Grinzato, Thermal diffusivity measurement in slabs using harmonic and one dimensional propagation of thermal waves, Int. J. Therm. Sci. 43 (5) (2004) 453–463.

- [104] P. Bison, S. Marinetti, A. Mazzoldi, E. Grinzato, C. Bressan, Cross comparison of thermal diffusivity measurements by thermal methods, Infrared Phys. Technol. 43 (3–5) (2002) 127–132.
- [105] P. Bison, F. Cernuschi, E. Grinzato, In depth and in plane thermal diffusivity measurements of thermal barrier coatings by ir camera: evaluation of ageing, Int. J. Thermophys. 29 (6) (2008) 2149–2161.
- [106] G. Ferrarini, P. Bison, A. Bortolin, G. Cadelano, Thermal response measurement of building insulating materials by infrared thermography, Energy Build. 133 (2016) 559–564.
- [107] P. Bison, G. Cadelano, E. Grinzato, Thermographic signal reconstruction with periodic temperature variation applied to moisture classification, Quant. InfraRed.Thermogr.J 8 (2) (2011) 221–238.
- [108] International Organization for Standardization (ISO), Thermal Insulation. Qualitative Detection of Thermal Irregularities in Building Envelopes. Infrared Method, Standard Iso 6781., Genève: ISO, 2010.
- [109] European Committee for Standardization (Cen), thermal performance of buildings. qualitative detection of thermal irregularities in building envelopes, infrared method, standard en 13187, CEN, Brussels, 1998.
- [110] T.I. Ward, G. Hannah, C.H. Sanders, Conventions for Calculating Linear Thermal Transmittance and Temperature Factors, IHS BRE Press, 2016.
- [111] T.I. Ward, Assessing the Effects of Thermal Bridging at Junctions and Around Openings, vol. 1, 2006.
- [112] T. Taylor, J. Counsell, S. Gill, Combining thermography and computer simulation to identify and assess insulation defects in the construction of building façades, Energy Build. 76 (2014) 130–142.
- [113] A. Tavukçuoğlu, A. Düzgüneş, E. Caner Saltık, Ş. Demirci, Use of ir thermography for the assessment of surface water drainage problems in a historical building, ağzıkarahan (aksaray), turkey, NDT & E International 38 (5) (2005) 402–410.
- [114] S. Ribarić, D. Marčetić, D.S. Vedrina, A knowledge based system for the non destructive diagnostics of façade isolation using the information fusion of visual and ir images, Expert Syst. Appl. 36 (2) (2009) 3812–3823.
- [115] V.P. Vavilov, A pessimistic view of the energy auditing of building structures with the use of infrared thermography, Russ. J. Nondestr. Test. 46 (12) (2010) 906–910.
- [116] E. Bauer, E. Pavon, E. Barreira, E.K. De Castro, Analysis of building facade defects using infrared thermography: laboratory studies, J. Build Eng. 6 (2016) 93–104.
- [117] S. Bagavathiappan, B. Lahiri, T. Saravanan, J. Philip, T. Jayakumar, Infrared thermography for condition monitoring a review, Infrared Phys. Technol. 60 (2013) 35–55.
- [118] T. Kalamees, Air tightness and air leakages of new lightweight single-family detached houses in Estonia. Build. Environ. 42 (6) (2007) 2369–2377.
- [119] J. Hart, A practical guide to infra red thermography for building surveys, Building Research Establishment (1991) 1–98.
- [120] International organization for standardization (iso), Thermal Performance of Renewable and Sustainable Energy Reviews 82 (2018) 3077 30903089 Buildings. Determination of Air Permeability of Buildings. Fan Pressurization method., Standard ISO 9972, Bruxelles: ISO, 2006.
- [121] R. Albatici, A.M. Tonelli, Infrared thermovision technique for the assessment of thermal transmittance value of opaque building elements on site, Energy Build. 42 (11) (2010) 2177–2183.
- [122] G. DallÓ, L. Sarto, A. Panza, et al., Infrared screening of residential buildings for energy audit purposes: results of a field test, Energies 6 (8) (2013) 3859–3878.
- [123] I. Nardi, S. Sfarra, D. Ambrosini, Quantitative thermography for the estimation of the u value: state of the art and a case study, in: Journal of Physics: Conference Series, vol. 547, IOP Publishing, 2014, 012016.
- [124] I. Nardi, D. Paoletti, D. Ambrosini, T. de Rubeis, S. Sfarra, Validation of quantitative ir thermography for estimating the u value by a hot box apparatus, in: Journal of Physics: Conference Series, vol. 655, IOP Publishing, 2015, 012006.
- [125] R. Albatici, A.M. Tonelli, M. Chiogna, A comprehensive experimental approach for the validation of quantitative infrared thermography in the evaluation of building thermal transmittance, Appl. Energy 141 (2015) 218–228.
- [126] R. Madding, Finding r values of stud frame constructed houses with ir thermography, Proc. InfraMation 2008 (2008) 261–277.
- [127] Y. Ham, M. Golparvar Fard, 3d visualization of thermal resistance and condensation problems using infrared thermography for building energy diagnostics, Visual. Eng. 2 (1) (2014) 12.
- [128] L. Ibos, J.P. Monchau, V. Feuillet, Y. Candau, A comparative study of in situ measurement methods of a building wall thermal resistance using infrared thermography, in: Twelfth International Conference on Quality Control by Artificial Vision 2015, vol. 9534, International Society for Optics and Photonics, 2015, p. 953411.
- [129] C. Ghiaus, Experimental estimation of building energy performance by robust regression, Energy Build. 38 (6) (2006) 582–587.
- [130] R.D.L. Vollaro, C. Guattari, L. Evangelisti, G. Battista, E. Carnielo, P. Gori, Building energy performance analysis: a case study, Energy Build. 87 (2015) 87–94.
- [131] J. Kim, J. Lee, J. Kim, C. Jang, H. Jeong, D. Song, Appropriate conditions for determining the temperature difference ratio via infrared camera, Build. Serv. Eng. Technol. 37 (3) (2016) 272–287.
- [132] S. Kato, K. Kuroki, S. Hagihara, Method of in situ measurement of thermal insulation performance of building elements using infrared camera, in: 6th International Conference on Indoor Air Quality, Ventilation & Energy Conservation in Buildings IAQVEC, vol. 2007, 2007. Citeseer.
- [133] E. Grinzato, P. Bison, G. Cadelano, F. Peron, R value estimation by local thermographic analysis, in: Thermosense XXXII, vol. 7661, International Society for Optics and Photonics, 2010, p. 76610H.

- [134] J. Thouvenel, Find a Modern and Quick Method to Determine the U Value and the Thermal Characteristics of a Building Envelope Using an Ir Camera, 2012.
- [135] Y. Ham, M. Golparvar Fard, Automated cost analysis of energy loss in existing buildings through thermographic inspections and cfd analysis, in: ISARC. Proceedings of the International Symposium on Automation and Robotics in Construction, vol. 30, Vilnius Gediminas Technical University, Department of Construction Economics, 2013, p. 1.
- [136] K. Ohlsson, T. Olofsson, Quantitative infrared thermography imaging of the density of heat flow rate through a building element surface, Appl. Energy 134 (2014) 499–505.
- [137] I. Simões, N. Simões, A. Tadeu, J. Riachos, Laboratory assessment of thermal transmittance of homogeneous building elements using infrared thermography, in: Proceedings of the 12th International Conference on Quantitative InfraRed Thermography, France, Bordeaux, 2014, pp. 7–12.
- [138] V. Tzifa, G. Papadakos, A. Papadopoulou, V. Marinakis, J. Psarras, Uncertainty and method limitations in a short time measurement of the effective thermal transmittance on a building envelope using an infrared camera, Int. J. Sustain. Energy (2014) 1–19.
- [139] I. Nardi, D. Paoletti, D. Ambrosini, T. De Rubeis, S. Sfarra, U value assessment by infrared thermography: a comparison of different calculation methods in a guarded hot box, Energy Build. 122 (2016) 211–221.
- [140] B. Tejedor, M. Casals, M. Gangolells, X. Roca, Quantitative internal infrared thermography for determining in situ thermal behaviour of façades, Energy Build. 151 (2017) 187–197.
- [141] A. Marshall, J. Francou, R. Fitton, W. Swan, J. Owen, M. Benjaber, Variations in the u value measurement of a whole dwelling using infrared thermography under controlled conditions, Buildings 8 (3) (2018) 46.
- [142] T. Kisilewicz, A. Wrobel, Quantitative infrared wall inspection, in: proceeding of 10th international conference on quantitative InfraRed thermography, Quebec, du CAO, Les Eboulements (2010) 78–81.
- [143] I. Nardi, D. Ambrosini, D. Paoletti, S. Sfarra, Combining infrared thermography and numerical analysis for evaluating thermal bridges in buildings: a case study, Int. J. Eng. Res. Afr. 5 (2015) 67–76.
- [144] M. OGrady, A.A. Lechowska, A.M. Harte, Quantification of heat losses through building envelope thermal bridges influenced by wind velocity using the outdoor infrared thermography technique, Appl. Energy 208 (2017) 1038–1052.
- [145] M. O'Grady, A.A. Lechowska, A.M. Harte, Infrared thermography technique as an in situ method of assessing heat loss through thermal bridging, Energy Build. 135 (2017) 20–32.
- [146] G. Baldinelli, F. Bianchi, A. Rotili, D. Costarelli, M. Seracini, G. Vinti, F. Asdrubali, L. Evangelisti, A model for the improvement of thermal bridges quantitative assessment by infrared thermography, Appl. Energy 211 (2018) 854–864.
- [147] C. Boué, S. Holé, Infrared thermography protocol for simple measurements of thermal diffusivity and conductivity, Infrared Phys. Technol. 55 (4) (2012) 376–379.
- [148] S. Dudić, I. Ignjatović, D. Šešlija, V. Blagojević, M. Stojiljković, Leakage quantification of compressed air using ultrasound and infrared thermography, Measurement 45 (7) (2012) 1689–1694.
- [149] M.B. Dufour, D. Derome, R. Zmeureanu, Analysis of thermograms for the estimation of dimensions of cracks in building envelope, Infrared Phys. Technol. 52 (2–3) (2009) 70–78.
- [150] G. Desogus, S. Mura, R. Ricciu, Comparing different approaches to in situ measurement of building components thermal resistance, Energy Build. 43 (10) (2011) 2613–2620.
- [151] T. Tiihonen, Stefan Boltzmann radiation on non convex surfaces, Math. Methods Appl. Sci. 20 (1) (1997) 47–57.
- [152] R. Albatici, F. Passerini, A.M. Tonelli, S. Gialanella, Assessment of the thermal emissivity value of building materials using an infrared thermovision technique emissometer, Energy Build. 66 (2013) 33–40.
- [153] S.J. Kim, S.W. Lee, Air cooling technology for electronic equipment, CRC press (1996) 1–272.
- [154] M. Gaši, B. Milovanović, S. Gumbarević, Infrared thermography for dynamic thermal transmittance determination, in: International Conference on Sustainable Materials, Systems and Structures (SMSS 2019) Energy Efficient Building Design and Legislation, 2019.
- [155] W. Chow, K. Chan, Parameterization study of the overall thermal-transfer value equation for buildings, Appl. Energy 50 (3) (1995) 247–268.
- [156] T.P. Wutka, H. Bryan, Overview of standard 90.1, ASHRAE J. 32 (2) (1990) 26–32.
- [157] W. Chow, P.C. Yu, Comment on the overall thermal transfer value (ottv) for building energy control, J. Architect. Eng. 4 (4) (1998) 149–154.
- [158] W. Chow, C. Philip, Controlling building energy use by overall thermal transfer value (ottv), Energy 25 (5) (2000) 463–478.
- [159] P.-b. B. E. Code, Electrical and Mechanical Services Department, Government of Hong Kong Special Administrative Region, 2007.
- [160] E. Sowell, Load calculations for 200,640 zones, Build. Eng. 94 (1988) 716–736.
- [161] E. Sowell, Classification of 200,640 parametric zones for cooling load calculations, Build. Eng. 94 (1988) 754–777.

- [162] S.M. Harris, Study to Categorize Walls and Roofs on the Basis of Thermal Response, Ph.D. thesis, Oklahoma State University, 1988.
- [163] W. Sheng, L. Zhang, I. Ridley, The impact of minimum ottv legislation on building energy consumption, Energy Pol. 136 (2020) 111075.
- [164] P. Tummu, S. Chirarattananon, V.D. Hien, P. Chaiwiwatworakul, P. Rakkwamsuk, Formulation of an ottv for walls of bedroom in Thailand, Appl. Therm. Eng. 113 (2017) 334–344.
- [165] Y.-H. Lin, K.-T. Tsai, M.-D. Lin, M.-D. Yang, Design optimization of office building envelope configurations for energy conservation, Appl. Energy 171 (2016) 336–346.
- [166] M.-D. Yang, M.-D. Lin, Y.-H. Lin, K.-T. Tsai, Multiobjective optimization design of green building envelope material using a non-dominated sorting genetic algorithm, Appl. Therm. Eng. 111 (2017) 1255–1264.
- [167] J. Yu, L. Tian, X. Xu, J. Wang, Evaluation on energy and thermal performance for office building envelope in different climate zones of China, Energy Build. 86 (2015) 626–639.
- [168] S. Goel, R.A. Athalye, W. Wang, et al., Enhancements to ashrae standard 90.1 prototype building models, Tech. rep., Pacific Northwest National Lab. (PNNL), Richland, WA (United States) (2014) 1–59. PNNL-23269.
- [169] A. Standard, Standard 90–1975, Energy Conservation in New Building Design, 1975
- [170] J. Lee, S. Kim, J. Kim, D. Song, H. Jeong, Thermal performance evaluation of low-income buildings based on indoor temperature performance, Appl. Energy 221 (2018) 425–436.
- [171] A. Council, Energy efficiency building standards in Japan, Acesso em março (2007) 1–9.
- [172] S. Vidas, P. Moghadam, Heatwave: a handheld 3d thermography system for energy auditing, Energy Build. 66 (2013) 445–460.
- [173] G. Baldinelli, F. Bianchi, Windows thermal resistance: infrared thermography aided comparative analysis among finite volumes simulations and experimental methods, Appl. Energy 136 (2014) 250–258.
- [174] K. Maroy, K. Carbonez, M. Steeman, N. Van Den Bossche, Assessing the thermal performance of insulating glass units with infrared thermography: potential and limitations, Energy Build. 138 (2017) 175–192.
- [175] A. Krenzinger, A. de Andrade, Accurate outdoor glass thermographic thermometry applied to solar energy devices, Sol. Energy 81 (8) (2007) 1025–1034.
- [176] F. Cerdeira, M. Vázquez, J. Collazo, E. Granada, Applicability of infrared thermography to the study of the behaviour of stone panels as building envelopes, Energy Build. 43 (8) (2011) 1845–1851.
- [177] C. Meola, Infrared thermography of masonry structures, Infrared Phys. Technol. 49 (3) (2007) 228–233.
- [178] C. Meola, R. Di Maio, N. Roberti, G.M. Carlomagno, Application of infrared thermography and geophysical methods for defect detection in architectural structures, Eng. Fail. Anal. 12 (6) (2005) 875–892.
- [179] F. Ascione, N. Bianco, R.F. De Masi, F. de Rossi, G.P. Vanoli, Simplified state space representation for evaluating thermal bridges in building: modelling, application and validation of a methodology, Appl. Therm. Eng. 61 (2) (2013) 344–354.
- [180] F. Bianchi, A. Pisello, G. Baldinelli, F. Asdrubali, Infrared thermography assessment of thermal bridges in building envelope: experimental validation in a test room setup, Sustainability 6 (10) (2014) 7107–7120.
- [181] L. Zalewski, S. Lassue, D. Rousse, K. Boukhalfa, Experimental and numerical characterization of thermal bridges in prefabricated building walls, Energy Convers. Manag. 51 (12) (2010) 2869–2877.
- [182] https://www.wunderground.com/.
- [183] https://supervise.ly/.
- [184] A. Verma, P. Singh, J.S.R. Alex, Modified convolutional neural network architecture analysis for facial emotion recognition, in: 2019 International Conference on Systems, Signals and Image Processing (IWSSIP), IEEE, 2019, pp. 169–173.
- [185] P. Bharati, A. Pramanik, Deep learning techniques-r-cnn to mask r-cnn: a survey, in: Computational Intelligence in Pattern Recognition, Springer, 2020, pp. 657–668.
- [186] Y. Yu, K. Zhang, L. Yang, D. Zhang, Fruit detection for strawberry harvesting robot in non-structural environment based on mask-rcnn, Comput. Electron. Agric. 163 (2019) 104846.
- [187] T. Rakha, A. Gorodetsky, Review of unmanned aerial system (uas) applications in the built environment: towards automated building inspection procedures using drones, Autom. ConStruct. 93 (2018) 252–264, https://doi.org/10.1016/j. autcon.2018.05.002. http://www.sciencedirect.com/science/article/pii/S0 926580518300165.
- [188] M.H. Shariq, B.R. Hughes, Revolutionising building inspection techniques to meet large-scale energy demands: a review of the state-of-the-art, Renew. Sustain. Energy Rev. 130 (2020) 109979.
- [189] Youness Arjoune, Sai Peri, Niroop Sugunaraj, Debanjan Sadhukhan, Michael Nord, Gautham Krishnamoorthy, David Flynn, Prakash Ranganathan, Thermal imagery based instance segmentation for energy audit applications in buildings, in: 2019 IEEE International Conference on Big Data (Big Data), 2019, pp. 5974–5976.